Effect of pH on the Langmuir monolayers of Zirconyl Stearate and the synthesized Zirconium Oxide thin films

A thesis

Submitted in partial fulfillment of the requirement for the award of degree of

MASTER OF SCIENCE

in

PHYSICS

Submitted by

Raveena Choudhary

(Roll No. 301504027)

Under the guidance of
Dr. Loveleen K. Brar
Assistant Professor

School Of Physics And Materials Science
Thapar University, Patiala– 147004

July- 2017

Dedicated to

My Family and Dr. Loveleen K. Brar

For their love and support

Certification

I hereby certify that this thesis entitled, **"Effect of pH on the Langmuir monolayers of Zirconyl Stearate and the synthesized Zirconium Oxide thin films"** in partial fulfillment for the requirements for the award of Degree of Master of Science in Physics submitted to School of Physics and Materials Science, Thapar University, Patiala, is an authentic record of my own work and is carried under the supervision of **Dr. Loveleen K. Brar**. The matter submitted via this thesis report has not been submitted for the award of any other degree to the best of our knowledge.

Date: 21 Aug, 2017
Place: Thapar University, Patiala

Raveena
(301504027)

This is to certify that the above statement made by the candidate is correct and true to the best of my knowledge.

Dr. Loveleen K. Brar.
Assistant Professor
Thapar University, Patiala-147004

Acknowledgements

First and foremost, I would like to express my sincere and deepest appreciation to my M.Sc. dissertation thesis supervisor, **Dr. Loveleen K. Brar** Assistant Professor, SPMS, Thapar University, Patiala - 147004, India for her valuable discussions and suggestions, guidance, strong motivation, encouragement and inspiration throughout my M.Sc. dissertation thesis journey.

I also express my heartiest gratitude to **Dr. Manoj Kumar Sharma**, Head and Professor, School of physics and materials science, Thapar University, Patiala - 147004, India for his support throughout the period.

A special thanks to **Ms. Rajni Sharma** and **Ms. Palvi Pruthi** for their valuable guidance in learning technique.

I would like to thank **SAI Labs Thapar University, SAIF Punjab University, Chandigarh** for doing characterization techniques.

I am thankful to **Ms. Amanpreet Kaur**, **Ms. Rajpal Kour** for helping me in performing experiments and analyzing the data.

I would like to express my deepest gratitude to my beloved grandparents **Mr. G.R. Khicher** and **Mrs. Jhumar Devi.** My parents, **Mr. Vijay Kumar** and **Mrs. Kavita Choudhary** and younger brother **Mr. Vipin Choudhary,** who have always believed in me, and endured with me during difficult times.

I would like to express my love to my best friend, **Ms. Renuka Saharan** who inspires me every day to be strong and keep me going with her smile and love.

Last but not least, deepest thanks to all the friends who have always been with me.

Date: ~~June~~ 21 August, 2017

Raveena

Abstract

Zirconium oxide is a very important material from applications point of view finds applications in coatings and as oxygen sensor. The control of thickness, roughness and surface morphology are some of the important parameters which need to be controlled. Langmuir-Blodgett (LB) thin film deposition method is known for the precise control of thin film parameters. In this work the thin uniform films of zirconium oxide were synthesized from the ZrO-stearate LB films. Characteristics of the Langmuir monolayers control the quality of LB films and the morphology of the final oxide thin film. ZrO-stearate Langmuir monolayers were deposited and characterized on the surface of the Langmuir trough. It was observed that at too low pH the ZrO^{2+} ions do not get incorporated in the monolayer. As the pH of subphase was increased the compaction of the film and its static elasticity in the solid phase was enhanced indicating an increase in ZrO^{2+} ion incorporation. An important result to emerge from these studies was that for very high pH (8.3) the structure of the films opens up. Analysis of π-A isotherms showed that pH 7.3 monolayer has good parameters for the LB deposition. Cyclic compression and expansion of the monolayer showed that while the Mma reduces steadily, the static elasticity of the solid phase gets cycled. This behavior can be explained on the basis of the behavior of double bonded oxygen attached to the Zr atom. The oscillating barrier characterizations of ZrO-stearate monolayers at different frequencies and pH values were recorded. This characterization also confirmed the stability of the monolayers at pH 7.3. The LB films of ZrO-stearate were Z-type. The transparent Zirconium oxide thin films on glass substrate were synthesized by deposition of 9, 14, 20 layers of ZrO-stearate at 7.3 pH followed by drying, removal of stearate chain and calcination. The presence of Zr in the calcined films was checked by EDS. 15 layers deposited at pH 7.3 formed the best film with grain size of about 23 nm. The effect of pH on the final film morphology was determined by depositing 15 layers for 6.3, 7.9 and 8.3 pH values. The TR for the pH 6.3 and 8.3 monolayers was too low so the uniform films could not be deposited. For the pH 7.9 the deposition was possible but the final films have larger grain size and were more granular and uneven at local level.

Contents

List of Figures

List of Tables

Chapter 1

Introduction to zirconium oxide thin films

1.1 Thin films

A thin film is a layer of material having a thickness from fractions of a few nanometers to several micrometers [1]. Fig 1.1 showing a schematic diagram of thin film deposited on the substrate.

For a thin film, the two surfaces of the material are very close to one another so that they can have a conclusive influence on internal physical properties as well as processes of that substance which can now vary in an intense way from the bulk material. The small distance between the surfaces and their interaction results in the rise of a totally new conditions within the material. The reduction of one dimension of the material to an order of several atomic layers creates an intermediate system between macro systems and molecular systems, providing a method of investigation of the microphysical nature of various processes. The examples of thin film formation in nature are[1]:

- When we mix oil in water, a layer on the surface of water is formed.
- The wings of many insects act like thin films due to their thickness.
- The buttercup flowers appear glossy also due to a thin film.
- The breast feathers of birds of paradise also shine due to thin film on the surface.
- Bubble formation

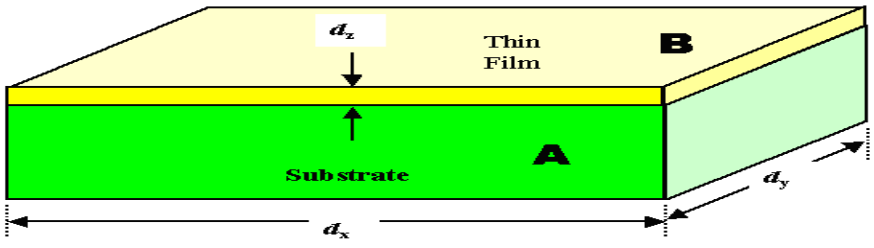

Fig 1.1 Showing schematic diagram of thin film deposited on a substrate [3]

Thin film materials are the essential elements of continued technology, applicable in almost all fields. The processing of Materials into thin films allows for easy unification into many types of devices. The properties of material appreciably differ when investigated in thin film form. Most of the functional materials are rather applied in the form of thin film due to

their specific electrical, magnetic and optical properties. Mostly, thin films are formed by deposition, both by physical and chemical methods. Both crystalline and amorphous thin films have huge importance in the current as well as a future era of high technology[2].

1.2 Importance of thin films

Thin films have great importance for a large variety of industrial applications. Some of them are wear and corrosion resistant coatings[40], which are able of extend the lifetime of a large no. of critical products. In addition, optical and electrically active, as well as magnetic thin films usually employed in sensors, solar cells, actuators, electro acoustic devices, nanocomposite porous films, etc. Technologies of thin films are continuously evolving for the fabrication of technologically advanced devices covering a wide spectrum of applications in different fields (fig 1.2)[1].

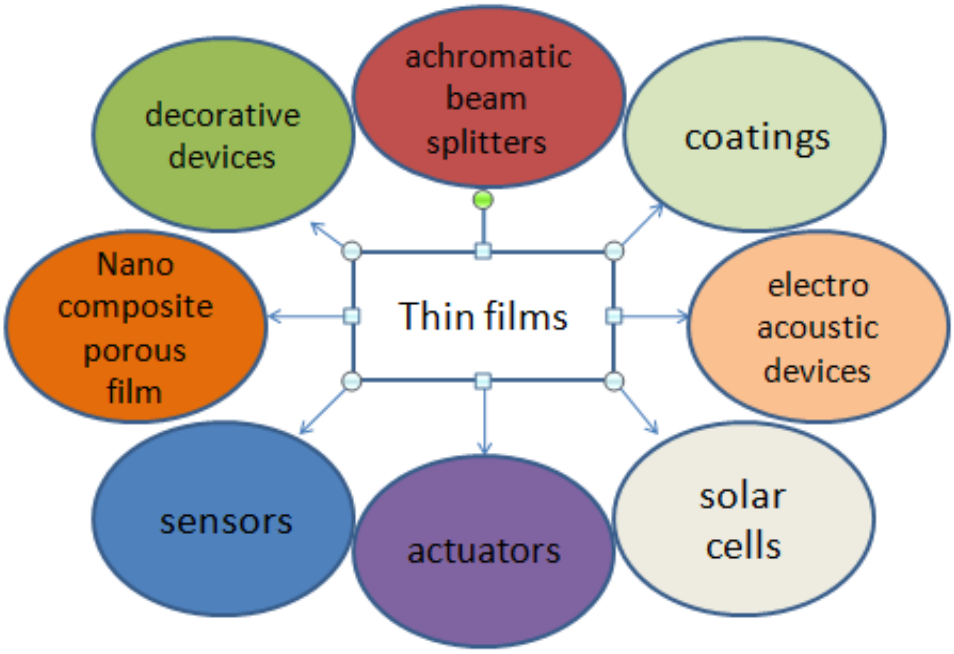

Fig 1.2 Technological significance of thin films.

1.3 Zirconium dioxide

Zirconium dioxide, also known as zirconium (ZrO_2), is a white crystalline oxide of zirconium. Its most naturally occurring form is a monoclinic crystalline structure[4]

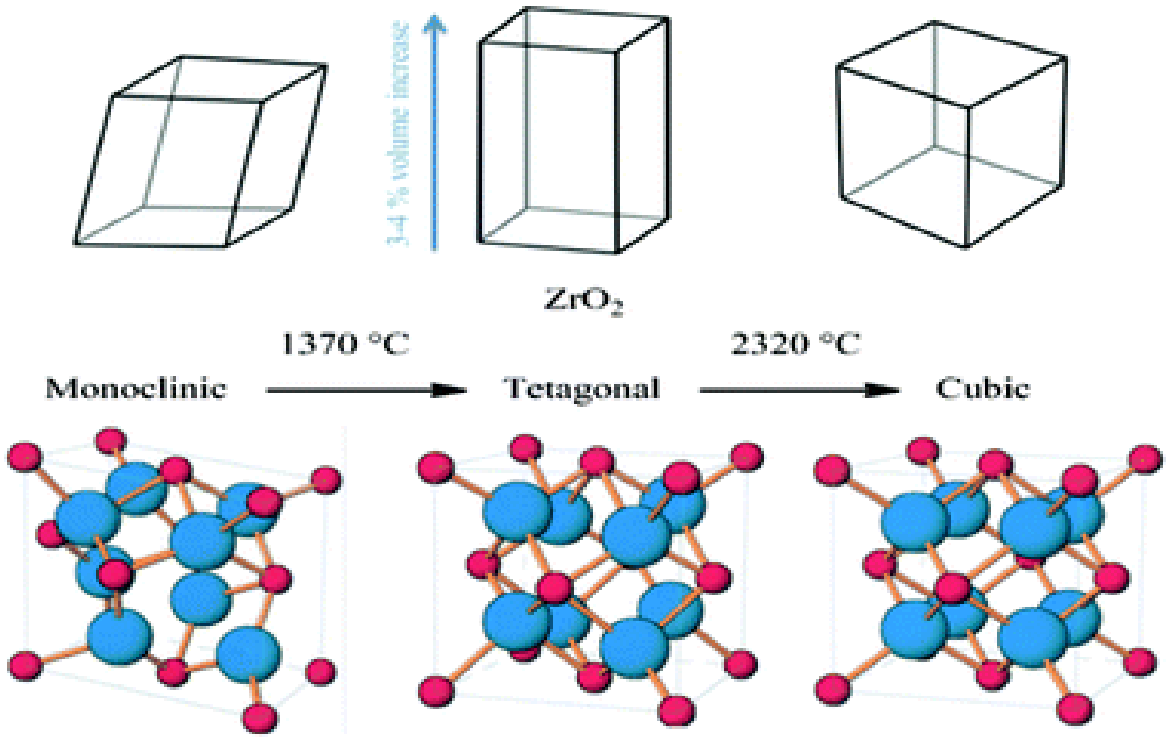

Fig 1.3 Structure of zirconium oxide[5]

Three phases are: monoclinic <1170 °C, tetragonal 1170–2370 °C, and cubic >2370 °C (fig 1.3)

Zirconia is chemically non reactive. Concentrated H_2SO_4 and HCl attacks on it slowly. Above 600 °C, it is electrically conducting and is used in the manufacture of high temperature furnaces. Zirconium oxide also has a very high thermal expansion as well as high strength. Zirconium oxide find applications in high refractive index coatings, high band gap and high thermal stability. A dopant stabilized cubic structured zirconia is synthesized in different colors and used as a gemstone and a diamond stimulant [4].

Table 1.1 Showing the properties of zirconium oxide [4]

Property	Value
Chemical formula	ZrO_2
Appearance	White powder
Cation	Zr^{4+}
Molar mass	123.218 g/mol
Solubility in water	Negligible
Density	5.68 g/cm^3
Band gap	5eV-7Ev
Dielectric Constant	~ 25
Lattice parameter	~2.5Å
Hardness	18 GPa for monoclinic phase 14 to 11 GPa for amorphous

1.4 Zirconium dioxide thin films

Zirconium oxide thin films are widely used in industry for optical and sensor applications. To prevent corrosion, thin films of ZrO_2 can be used in coatings and promotes thermal stability. In the form of thin films ZrO_2 is one of the most promising material systems having good mechanical, dielectric and Optical properties, which makes it suitable for application in catalysis, thermal barrier coatings, sensors, mirrors, fuel cells and microelectronics. Thin films of ZrO_2 can be grown by numerous techniques, which are thermal evaporation, sputtering, pulsed laser deposition (PLD), chemical vapor deposition (CVD) and atomic layer deposition (ALD), but most of these processes are complicated and uneconomic. The thickness of zirconia thin film varies from few Armstrong to several micrometers. Zirconium thin films can also be doped with materials such as iron, cobalt, nickel, zinc, yttrium, lanthanum, manganese, germanium etc. resulting in modifying properties.

1.5 Properties of thin films of ZrO_2

- High Dielectric Constant (~25)
- Large resistance against oxidation
- Low thermal conductivity ($4.2 Wm^{-1}K^{-1}$)
- High thermal stability

- High refractive index (2.2)
- Barrier heights of about 1.5 eV with respect to silicon besides low achievable trap densities
- Broad spectral region of low absorption from 240 nm to 8 μm
- Good adhesion to substrates

1.6 Applications of thin films of ZrO_2

Thin films of ZrO_2 have a vast range of applications[6]:

- Anti reflection coatings, achromatic and color selective beam splitters.
- Coating material for corrosion as well as oxidation, electronic devices, highly refractive mirrors, decorative devices.
- In oxygen gas sensors
- Fuel cells of high temperature.
- Planar waveguide materials as hosts for lasers and OP-AMPs.
- In passive thin film materials (Resistors, Condensers, Interconnects) and active thin film materials (Transistors, Diodes)
- Neurological sensors and biocamptible implant coatings
- Hard coatings for cutting tools and catalyzing coatings in engineering and processing.
- Bone marrow stem cells are found to grow and spread in good states on the ZrO_2 thin film surface.

1.7 References

1. M. Ohring (2001). Materials Science of Thin Films (2nd ed.). Boston: Academic Press
2. G. Roberts, Ed. Langmuir Blodgett films, plenum press: New York, (1990)
3. J.S. Peng, W. Fang, H. Y. Lin, C.H. Hsueh, S. Lee, *J. Micromech. Microeng,* 23(2013) 095001
4. R. Stevens, 1986. Introduction to Zirconia. Magnesium Elektron Publication No 113
5. J. P. Abarog, C.-Lise, A. Crochet, K.M. Fromm, *ChemPhysChem,* 3(2013), 16905-16931
6. D. Panda, T.-Y. Tseng, *Thin Solid Films*, 531(2013), 1-20

Chapter 2

Langmuir-Blodgett

2.1 Langmuir-Blodgett technique

When a monolayer is formed at the air-aqueous or aqueous-aqueous surface, we call that thin film as Langmuir film. When we deposit a Langmuir film on any solid substrate, it is known as Langmuir-Blodgett (LB) film. The basic idea of this method is to form a monolayer of an amphiphillic material on the surface of water and then transferring it on a solid substrate [1].

Some concepts from surface chemistry related to the LB technique are explained in the following sections.

2.2 Surface tension

To reduce their free energy, amphiphillic molecules orient themselves at the interface between a liquid and gaseous phase. The surface film formed having thickness of one molecule and is generally known as a monomolecular layer or monolayer. The surface molecules do experience net inward force as the forces on them are not like that of the bulk molecules. The linear force which acts on the surface molecules is known as surface tension Υ. The surface tension is affected by the pressure of a monolayer on a liquid surface. In monolayer experiments generally surface pressure is measured[2]. The surface pressure π is equal to reduction in the surface tension of the pure liquid due to the film, i.e.

$$\pi = \Upsilon_0 - \Upsilon$$

Υ_0 = Surface tension of the liquid surface

Υ = Surface tension of the liquid surface covered with film.

2.3 Amphiphilic molecules

Amphiphilic molecules contain both hydrophilic (water loving) as well as hydrophobic group (fat loving). They are having long hydrocarbon chains from 4 to 22 or more carbon atoms. All the fatty acids are amphiphiles. Steraic acid is one of the example of amphiphile.

When a solution of stearic acid and water-immiscible solvent like chloroform is poured on the water surface, the solution spreads instantly to cover the free area. As the solvent

evaporates, a monolayer is formed with the head groups dipped in the water surface with the tailgroups remaining outside (fig 2.1) [2].

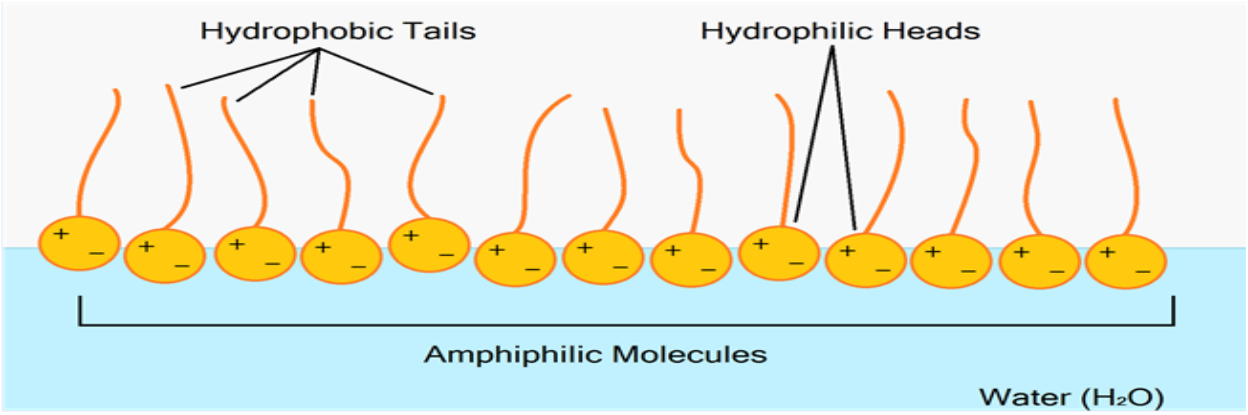

Fig 2.1 Amphiphilic molecule in water [3]

2.4 Surface pressure-area isotherms

The necessary measure of the monolayer properties of any material is given by surface pressure plotted against the area of subphase available to each molecule. This is carried out at a constant temperature and thus known as a surface pressure/area isotherm.

A number of regions, called phases, appear during the analysis of the isotherms. In gaseous phase, molecules are far away on the surface of subphase, thus exerting a little force on each other. The hydrocarbon chain will start interacting and liquid state is formed when the surface area reduced from its initial value, the phase is called expanded phase (fig 2.2). On further reduction of molecular area, a condensed phase appears (also called solid phase). Which follows a sudden transition to a steeply sloping linear region, where the compressibility is given by the equation [1].

$$\mathbf{C} = \frac{-1}{\mathbf{A}} \frac{d\mathbf{A}}{d\Pi} \qquad \text{.....(2.1)}$$

At constant T.

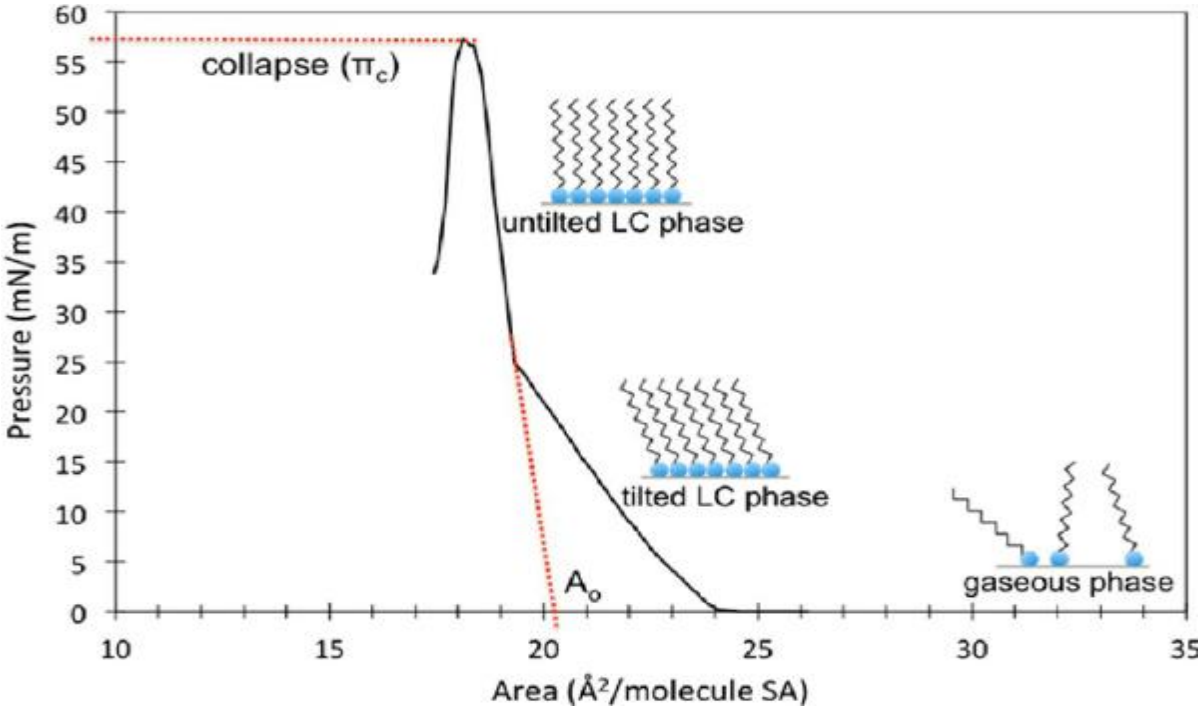

Fig 2.2 Surface pressure area isotherm [4]

In still smaller surface areas, due to collapse of monolayer, the compressibility becomes approximately infinite.

2.5 Effect of pH of subphase

Stearic acid is an amphiphilc molecule. When spread on a liquid subphase, the water soluble part gets ionized and its H^+ ion splits out and =o-o^- part remains with the molecule as shown in fig 2.3:

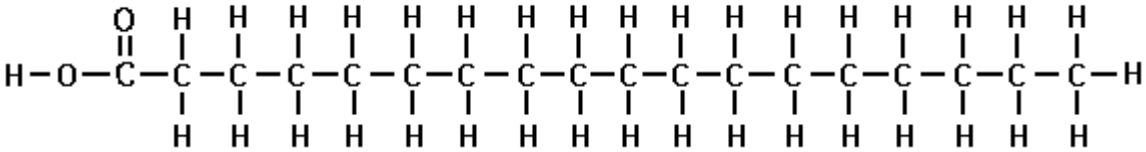

Fig 2.3 Structure of stearic acid [5]

Now, if subphase contains the ions, they will get attached to the ionized stearic acid and a monolayer of metal stearate will form. The ionization and hence the metal incorporation is subphase pH dependent. Incorporation of divalent metal ions increases the stability of the

film. But if pH would be increased above a certain limit,maximum metal ions will incorporate and due to nearness they start repel each other (fig 2.4) [28].

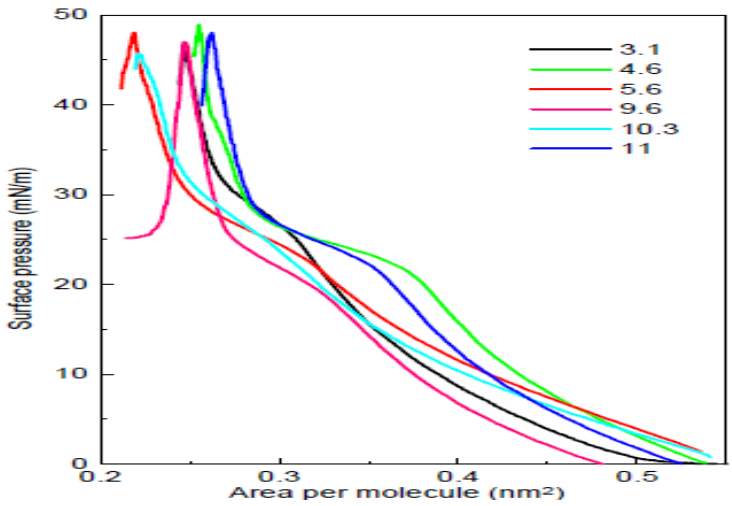

Fig 2.4 Surface pressure area isotherm with different pH [6]

2.6 Hysteresis

Compression-expansion hysteresis is obtained by first compressing the film followed by expansion through a repeated number of cycles. Hysteresis is investigated to study the stability of the film formed. If monolayer will be stable, it would give a reproducible hysteresis (fig 2.5) and on the other hand, if the film formed is not stable, then there will not be any kind of hysteresis obtained [7].

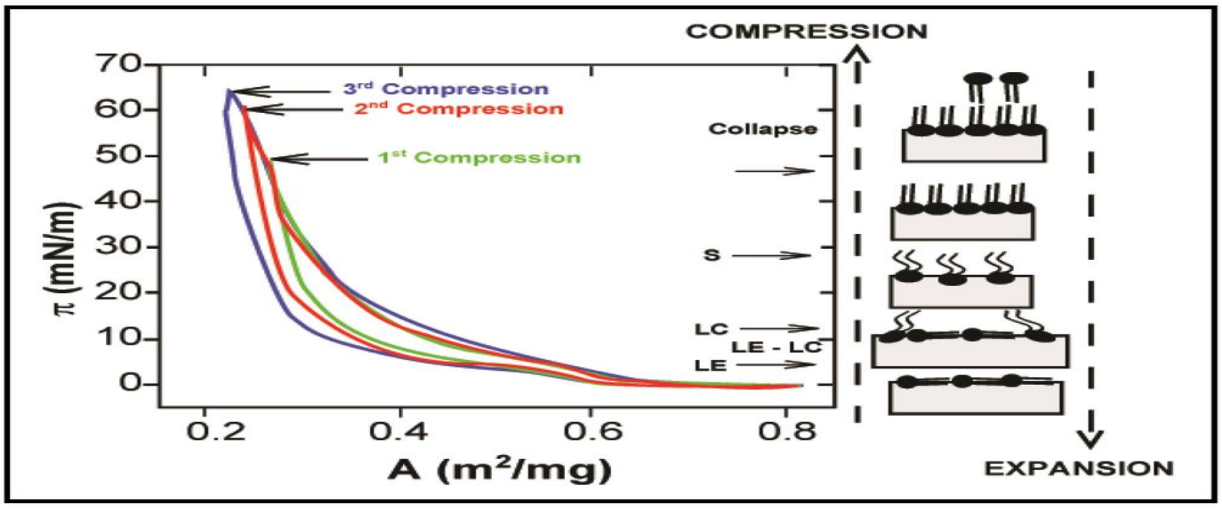

Fig 2.5 Hysteresis curve of the surface pressure area isotherm [8]

2.7 Oscillating Barriers

The visco-elastic properties of monolayer can be measured by oscillations of barriers, once the target pressure has been achieved. Dynamic visco-elastic properties like ε (dynamic elastic modulus), ε_s (storage elastic modulus) and ε_v(dissipation modulus) can be measured at those values of surface pressure at which phase change occurs. Studies of monolayers on oscillating barrier mode provide the most suitable surface pressure value for deposition [2]. Fig 2.6 shows time as a function of surface pressure and barrier position.

In this method, barriers start oscillating after achieving the target at a given frequency.

$$\boldsymbol{\varepsilon = \varepsilon_s + i\varepsilon_v} \qquad \text{.....(2.2)}$$

Where ε is complex quantity, ε_s is real part while $\varepsilon_v$is imaginary part.

Since, $\varepsilon_s = \varepsilon \cos\theta$ and $\varepsilon_v = \varepsilon \sin\theta$

$$\textbf{Loss angle} = \varepsilon_v/\varepsilon_s \qquad \text{.....(2.3)}$$

More condensed is the monolayer, more becomes its ε_v value and lesser becomes its ε value.

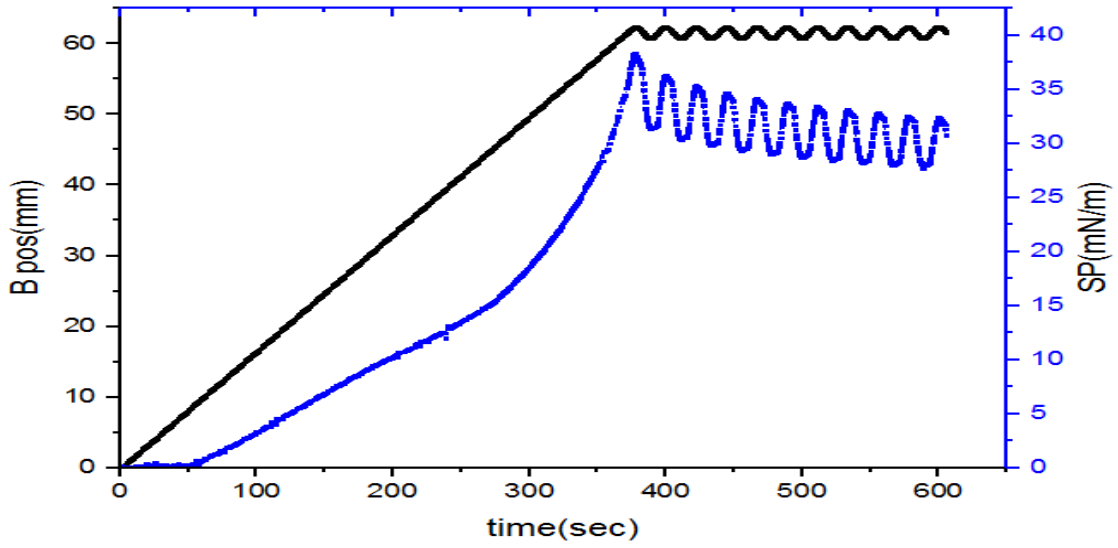

Fig 2.6 Graph showing time as a function of barrier position and π.

2.8 Experimental Setup of LB technique

In this part we will discuss about the experimental setup of the LB technique. The various parts of LB setup is shown in fig 2.7

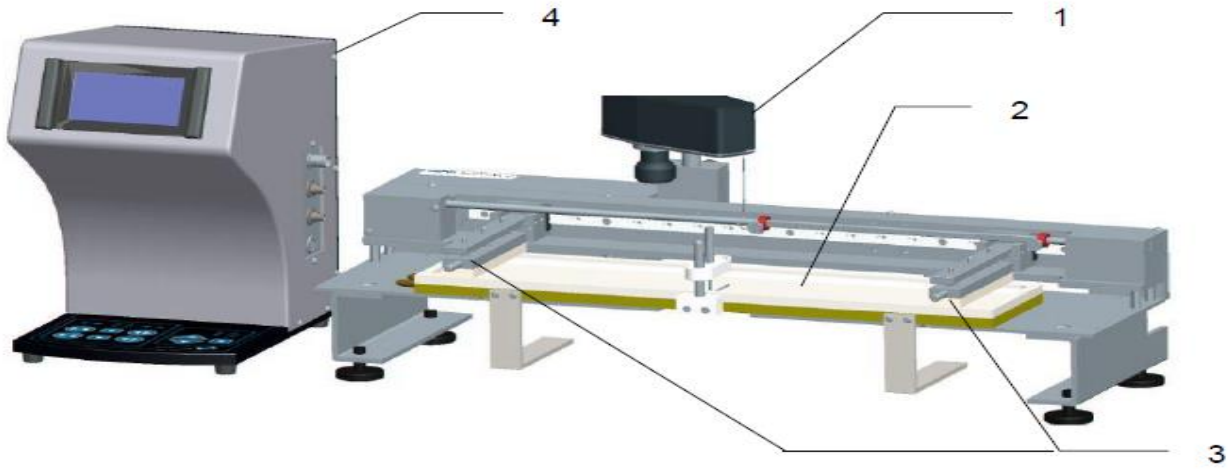

Fig 2.7 Langmuir-Blodgett setup [9]

1. Balance
2. Trough
3. Barriers
4. Layer builder

2.8.1 Trough: A Langmuir–Blodgett trough is a Teflon (hydrophobic and chemically inert) surface, used to compress the monolayers of molecules on the surface of a given subphase (usually water) and measure phenomena occur at surface. A monolayer of amphiphilic molecules on the surface of a liquid can be prepared on LB trough, and then compression or expansion of these molecules carried out at the surface, thereby modifying the area per molecule [9].

2.8.2 Substrates: A thin film substrate can be of two types i.e. hydrophilic and hydrophobic. Before thin film deposition, substrate should be cleaned using piranha cleaning. Also, it should be smooth for deposition of thin film.

The substrates which are used to deposit zirconia thin films are mainly glass, silicon, germanium, quartz etc.

2.8.3 Barriers: To compress or expand the monolayers, barriers slide parallel to the wall of the trough. The barriers are made out of teflon (hydrophobic material), due to which the film does not escape the barriers [9].

2.8.4 Wilhelmy plate: A Wilhelmy plate is a thin plate on the order of few square centimeters (fig 2.8), which is used to measure the equilibrium surface or interfacial

tension at an air–liquid interface. In this method, by hanging the plate perpendicular to interface, the force exerted on it can be measured. The plate is usually made of filter paper, glass or platinum. To ensure complete wetting, plate may be roughened [9].

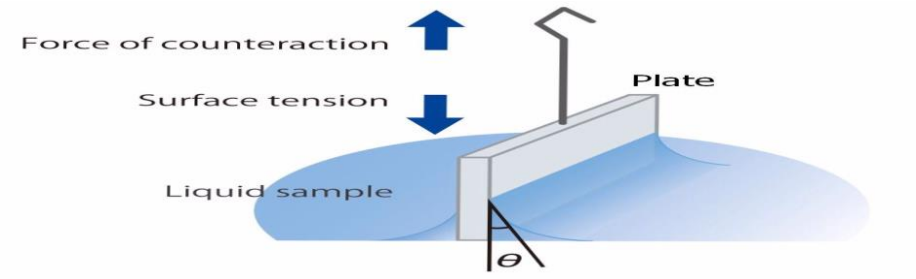

Fig 2.8 A wilhelmy plate [9]

2.8.5 Layer builder: A layer builder interface unit is connected to a computer and Most of the devices used with the LB are connected to it. The barrier drive, the balance, the dipper and other devices with 15-pin cables connect to the back of the layer builder interface unit [9].

2.9 Deposition of thin film

Stable Langmuir monolayer formed on the surface of subphase can be deposited on a substrate when a controlled surface pressure as well as temperature is attained and monolayer is in the solid phase (fig 2.9). Different types of substrates such as glass, silicon, quartz, etc. can be used and by dipping the solid substrate up and down while keeping the surface pressure constant through the computer feedback system, a number of monolayers can be deposited.

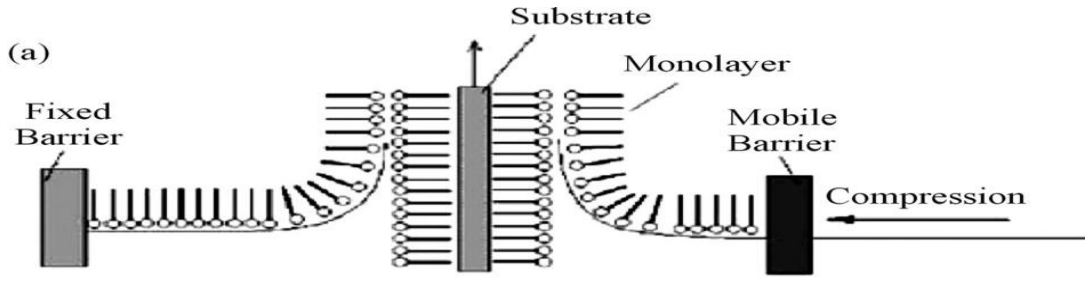

Fig 2.9 Transfer of thin film onto substrate [1]

The deposition of film is affected by parameters such as temperature, concentration, pH, nature of solvent, transfer process and nature of the solid substrate [2].

2.10 Types of deposition

Deposition of thin film on a substrate can take place by three ways X, Y and Z type deposition (fig 2.10) [2].

X-type deposition: This kind of deposition takes place only on a hydrophobic substrate and film deposits only by downstroke. This kind of deposition is used mostly for high pH values. Arrangement of molecules on the substrate is from head to tail.

Y-type deposition: The deposition is mainly depends upon the behavior of the substrate. In this case film deposit on a substrate by both upstroke and down stroke. The arrangement of molecules is in head to head and tail to tail pattern.

Z-type deposition: Sometimes, the monolayer are deposited only when the substrate is moving upwards the subphase i.e. upstroke and the films deposit on hydrophilic substrate only.

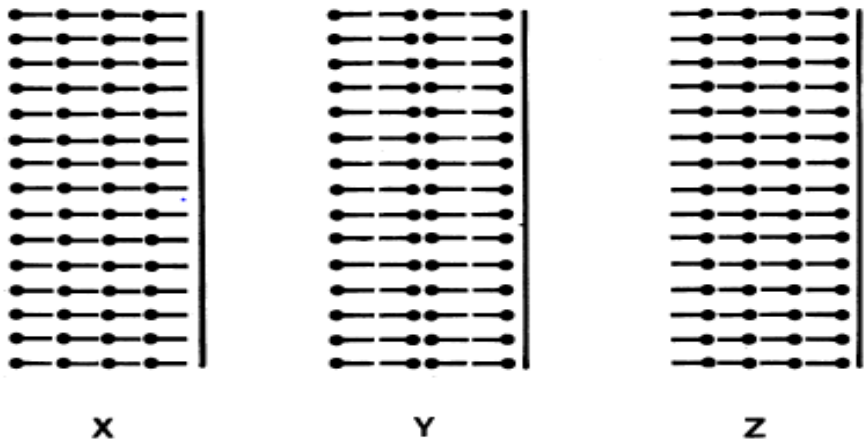

Fig 2.10 Types of deposition of thin films [1]

2.11 Transfer ratio

Transfer of the film is characterized by determining the deposition ratio or transfer ratio, τ. This is the ratio of decrease in area occupied by monolayer to that of the area of solid substrate on which film is deposited [1].

$$\tau = \frac{AL}{AS} \qquad \text{.....(2.4)}$$

The transfer ratio inside the range of 0.95 to 1.05 represents a good homogeneity of the deposited film.

2.12 References

1. G. Roberts, Ed. Langmuir Blodgett films, plenum press: New York, (1990)
2. Michael C. Petty. Handbook of Langmuir Blodgett Films, Cambridge University Press,(1996)
3. K. Panjabi, R. Rudra, *Open Journal of Civil Engineering*, 6 (2016), 13
4. E. C. Griffith, Teobaldo, R. C. Guizado, 117 (2013), *J. Phys. Chem*.117 (2013), 22341−22350
5. Seidell, Atherton; Linke, William F. (1919). Solubilities of Inorganic and Organic Compounds (2nd ed.). D. Van Nostrand Company
6. J. Nath, R. K. Nath, A. Chakraborty, and S. A. Husain, *Surf. Rev. Lett.,* 21 (2014), 1450049
7. C. J. L. Constantino, A. Dhanabalan, and O. N. Oliveira, *Review of Scientific Instruments* , 70 (1999), 3674
8. R. Pichot , R.L. Watson, *J. Mol. Sci*. 14 (2013), 11767-11794
9. Manual KSV NIMA Langmuir and Langmuir-Blodgett Deposition Troughs

Chapter 3

Literature review

Overview

In this chapter, we have discussed the papers studied during the literature survey. In the first section, we have discussed the papers related with various techniques to deposit zirconia films. In the remaining sections, we have discussed a few papers related to deposition of various thin films using the LB technique and hysteresis curve as well as oscillating barrier technique.

3.1 Synthesis of zirconium oxide thin films using various techniques

S. Venkataraj et al 2002 [1]. Zirconium oxide thin film of 175 nm was deposited on the glass and silicon substrate by reactive DC magnetron sputtering in the argon oxygen atmosphere. To investigate the variations in stoichiometry, structure, density, and optical properties on increasing oxygen partial pressure, the film was characterized with XRD, AFM, X-ray reflectometry, optical spectroscopy. From X-ray diffraction studies, the crystalline monoclinic structure of ZrO_2 films was observed, X-ray reflectivity determines a constant density of 6.5 g/cm^3 and a deposition rate of about 1.5 nm/s in the metallic mode.

B. O. Cho et al 2003 [2]. Zirconia thin films were deposited using a chemical vapor deposition technique on a p- type Si substrate to explain their tunable electrical properties. Without heating, the film obtained is of tetragonal phase and with an increase in O_2, it transformed into monoclinic phase. Also, with oxygen rich plasma, both dielectric constant and leakage current density decreased and interfacial layer formed as SiO_2. The interfacial thickness of film was found to be 2.7 nm and 5.4 nm with oxygen deficient and oxygen rich plasma respectively.

L. P. Borilo et al 2012 [3]. From zirconium oxochloride and ethanol FFSs, Zirconia thin films having thicknesses of 40-120 nm on deposited glass, silicon, quartz, polycor, and sapphire substrates. On glass or quartz substrates, film prepared are of amorphous structure but of crystalline structure when deposited on silicon, polycor, or sapphire. The refractive index is found 1.86–2.08 of the resulting ZrO_2 films, and are insulators, having bandgap width 5.0eV-5.2eV.

L. Sygellou et al 2012 [4]. Thin films of ZrO_2 and Al_2O_3 were prepared on p- type Ge substrate using atomic layer deposition technique. To investigate their chemical composition, thin films were analyzed using X ray photoelectron spectroscopy. The result verifies the formation of ZrO_2 and Al_2O_3 thin films along with OH group and carbon contamination on the surface. The ZrO_2 thin film was grown with a thickness of 20 nm and Al_2O_3 was of thickess 19 nm.

A. P. Kerasidou et al 2012 [5]. 5 and 25 nm thick ZrO_2 thin films were deposited by ALD at 250^0 C on a p type Ge substrate. Properties such as stoichiometry, thickness, and valence electronic band structure were investigated by X ray and UV photoelectron spectroscopies. The valance band edge is formed 4.1 eV below E_f, from J-V characteristics, it was concluded that in forward bias, the tunneling is a dominant conductivity mechanism and in reverse bias, the observed conductivity is attributed to the Poole-Frenkel mechanism.

Khojier et al 2013 [6]. Zirconium films of 90 nm thickness were deposited on glass substrate**,** by the method of direct current magnetron sputtering and then in constant flow of oxygen film was analyzed at various temperatures. From XRD, with annealing temparatures, it was observed that there is an increase in crystallite size and nanostrain The granular structure was observed with AFM. At higher temperatures, annealed films were gray but at low temperatures, they were brown in color. The applied voltage remained constant with variation in electrical resistance of the sample, while it is increased with annealing temperatures.

N. Jeyakumaran et al 2014 [7]. Zirconia thin films with 5,7,9 layers were prepared on glass substrates, using alcoholic solutions by method of sol gel dip coating. Sol gel derived films were heated at 500^0C after coating. From XRD data it was observed that monoclinic and tetragonal phases were formed at 500^0C and the grain size was found 2.25nm. From Photoluminescence studies, at 426nm, a strong emission peak and at 488nm, a weak emission peak were recorded.

3.2 Characterization of Langmuir films using Langmuir troughs

C. J. L. Constantino et al 1999 [8]. With the Wilhelmy method, the surface pressure was measured. By varying the conditions, such as change in the mode of compression, positioning of the wilhelmy plate, and compression speeds, the monolayer characteristics of lignins were analyzed. From experimental artifacts, a minimum in the decompression phase of a hysteresis experiment was arise, which are explained by the various forces experienced by the Wilhelmy plate.

H. Sakai et al 2001 [9]. On subphase (water), a Langmuir monolayer of zinc stearate and zinc-12 hydroxy stearate were formed. The structure about carboxylic group changes with the compression of zinc stearate but there is no change in orientation and confirmation hydrocarbon chain. Hence it was concluded that zinc-12 hydroxy stearate monolayers were different from that of the stearate monolayers.

D.Y. Zang et al 2010 [10]. The rheological behavior was investigated for silica nanoparticle monolayer at subphase surface. Both Langmuir monolayer and deposited layers were studied through Langmuir troughs. The compressed layers were found more rigid and homogeneous. and the deposited layers were less rigid, but more viscoelastic. From the oscillatory uniaxial compression, the shear moduli concluded are much smaller than those concluded from pure shear deformation specifying that the effective shear rate is lower than expected in the compression measurements.

R. Kaur et al 2013 [11]. By barrier oscillation, surface viscoelastic properties of FLC were studied and values of elastic modulus, storage modulus and loss modulus were determined. As the monolayer becomes condensed, values of ε_v increases while ε_s decreases. ε_v has negative values at higher frequencies. Study of monolayer in barrier oscillation modes provides the suitable surface pressure for deposition.

3.3 Deposition of Langmuir Blodgett thin films

L. Dziri et al 1998 [12]. The dipole interactions of the acetylcholinesterase (AChE) monolayer were studied at subphase surface, it was observed that the significant changes in the surface potential with pH changes are caused by inorganic groups of the enzymes. From AFM data, at low pH, an unfolding of the enzyme occurs forming large domains at

subphase instead of an organized AChE monolayer and the aggregates were formed by enzyme at high pH. The thickness of the monolayer was found to be 1 to 1.5 nm.

J. Nath et al 2008 [13]. The monolayer characteristics of a non-toxic and biodegradable polymer Chitosan (CHS) using the LB technique were investigated. The observation shows that a stable monlayer was not formed by pure CHS. But, if CHS is mixed with arachidic acid (AA), stable monolayer is formed at water surface which can also be transferred on a solid substrate. With the variation in pH, mixed monolayer is extremely stable. AFM study depicts the formation of stable, uniform CHS-AA films onto solid substrate and thickness varies from 13 to 30 nm with change in concentration of AA.

R. Kaur et al 2012 [14]. Monolayer of a ferroelectric liquid crystal (FLC) at water surface was deposited on quartz substrate using the LB technique. By compression, a stable monolayer of molecules on subphase formed. 11 and 22 layers were transferred to substrates by Y-type deposition and variation in thicknesses was observed. Low-angle X-ray diffraction shows smectic layering and FTIR spectroscopy confirmed complete deposition of FLC multilayers. The morphology of the monolayer was studied and analyzed by AFM.

N. Kumar et al 2012 [15]. By varying in concentration of Ca^{2+} and Na^{+} ions in subphase, their influences were compared on monolayers as well as deposited LB film. Stability and wettability of monolayer were studied using imaging ellipsometry, AFM and contact angle goniometry. It was concluded that SA binded Ca^{2+} much more efficiently with higher stability instead of Na^{+}. The thickness of monolayers was observed 2 nm.

N. Akhtar et al 2012 [16]. LB films formed as a mixture 1:2 of bis-(ethylenedioxy) tetrathiafulvalene (BEDO-TTF) and fatty acid and their structural and electrical properties were investigated. 22 layerd thick Langmuir–Blodgett films deposited on substrate shows better quality in terms of crystallinity as well as electrical conduction. Even at lower molar ratios, LB films with longer alkyl chain fatty acids were ordered better.

R. Kaur et al 2016 [17]. LB films of ferroelectric liquid crystal were prepared and characterized. Pressure–area isotherms indicate nano-particles and FLC composite systems from stable monolayer. There is an increase in the molecular interaction between nano particle and FLC during compression of barriers. Various change of phase with doping of nano-particles in the FLC matrix were observed. X-ray diffraction depicted that at low

concentration doping of nanoparticle, FLC retains its SmC structure. AFM images indicate that deposited composites do not disturb the translation behavior FLC and thickness varies from 7 nm to 20 nm with change in surface pressure.

3.4 Synthesis of oxide thin films using the LB technique

Z. Gang et al 2002 [18]. By using LB technique, Y_2O_3-stabilized ZrO_2 (YSZ) films of 400 layers were prepared. Metal complexes were incorporated with arachidic acid. From XRD and XPS,it was observed that the films formed are single phased fluorite cubic structure. It was also observed that the average grain size and morphology of film were affected by annealing temperature. The thickness of thin film was found to be 1.11 μm.

L. J. Cote et al 2008 [19]. The edge-to-edge and face-to-face geometries of single layer graphite oxide were studied at water surface by Langmuir-Blodgett method. Without any surfactant or stabilizing agent, Stable monolayers of graphite oxide single layers were obtained due to the strong electrostatic repulsion between the layers. The single layers get fold and wrinkle at edges to avoid collapsing into multilayers. The graphite oxide monolayers can be chemically reduced to graphene for electronic applications.

S. Sharma et al 2015 [20]. Thin films of nickel oxide (NiO) were prepared on Si substrate from LB technique. Using XPS spectroscopy, XRD and AFM, the deposition and structure were evaluated. The samples were annealed at different temperatures in vaccum. Sheet resistance was determined in terms of annealing temperature.

3.5 References

1. S. Venkataraj, O. Kappertz, H. Weis, R. Drese, R. Jayavel and M. Wuttig, *Journal of applied physics,* 92 (2002), 3599
2. B.O. Cho, J. P. Chang, J.-H. Min, S. H. Moon, Y. W. Kim and I. Levin, *J. Appl. Phys,* 93 (2003), 745–749
3. L. P. Borilo, L. N. Spivakova, *American Journal of Materials Science,* 2 (2012), 119-124
4. L. Sygellou, V. Gianneta, N. Xanthopoulos, D. Skarlatos, S. Georga, C. Krontiras, S. Ladas and S. Kennou, *Surf. Sci. Spectra*, 18 (2011), 58
5. A. P. Kerasidou, M. A. Botzakaki, *J. Vac. Sci. Technol. A Vacuum, Surfaces, Film,* 31 (2013), 126
6. K. Khojier, Hadi Savaloni and Fatemeh Jafari, Journal of Theoretical and Applied

Physics, (2013), 1-7

7. S. Jothi, N. Prithivikumaran and N. Jeyakumaran*, International Journal of ChemTech Research,* 6 (2014), 1971-1973

8. C. J. L. Constantino, A. Dhanabalan and O. N. Oliveira, *Rev. Sci. Instrum*, 70 (1999), 3674

9. H. Sakai, J. Umemura, *J*. Colloid Polym Sci, 280 (2002), 316-321

10. D. Y. Zang, E. Rio, D. Langevin, B. Wei and B. P. Binks, *Eur. Phys. J. E,* 31 (2010), 125–134

11. R. Kaur, G. K. Bhullar and K. K. Raina, *AIP Conf. Proc,* 36 (2013), 1377–1378

12. L. Dziri, S. Boussaad, N. Tao and R. M. Leblanc, *Thin Solid Films*, 327–329 (1998), 56–59

13. J. Nath, R. K. Nath, A. Chakraborty and S. A. Husain, *Surf. Rev. Lett,* 21 (2014), 1450049

14. R. Kaur, G. K. Bhullar and K. K. Raina, *Liq. Cryst*, 39 (2012), 1375–1380

15. N. Kumar, L. Wang, I. Siretanu, M. Duits and F. Mugele, *Langmuir*, 29 (2013), 5150–5159

16. N. Akhtar, R. Y. N. Gengler, T. T. M. Palstra and P. Rudolf, , *J. Phys. Chem. C* 116 (2012), 24130–24135

17. R. Kaur and K. K. Raina, *Ferroelectrics*, 495 (2016), 87–96

18. Z. Gang, F. Kun, H. Pingsheng and S. Haizeng, *Journal of Materials Chemistry, 12* (2002), 2998-3002

19. L. J. Cote, F. Kim and J. Huang, *J. Am. Chem. Soc* ,131 (2009), 1043–1049

20. S. Sharma, M. Kumar, S. Rani, D. Kumar and C.C. Tripathi, *nano letters,* 46 (2015), 3166-3172

Chapter 4

Materials and methods

Overview

In this chapter, the materials used during the synthesis and the methods used to perform the experiments and characterizations are discussed.

4.1 Materials

The following materials were used in this work:

1) **Zirconyl chloride octahydrate ($ZrOCl_2.8H_2O$):** It is used as a subphase material since it is a water soluble compound and was acquired from Sigma Aldrich (>98%).

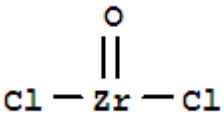

Fig 4.1 Structure of zirconyl chloride

2) **Stearic acid ($C_{17}H_{35}COOH$):** It is an organic acid with the property of forming a monolayer on the surface of water. The stearic acid which was used in experiments was a product of Sigma Aldrich (>98.5%).
3) **Chloroform ($CHCl_3$):** It evaporates quickly and is an organic solvent. So, in our experiments, we used chloroform to dissolve stearic acid and was bought from SDFCL (99%).
4) **Acetone (CH_3COCH_3):** It was used for cleaning glass slides, pH meter, microsyringe etc. and was a product of RANKEM (>99%).
5) **Methanol (CH_3OH):** In LB experiments, we used methanol as a cleaning reagent for trough and barriers and was acquired from SDFCL (HPLC grade)
6) **Propane-2-ol:** It was also used for cleaning of trough and barriers. It was acquired from fisher scientific (=99.7%).
7) **Deionized water:** Deionized water was used in subphase preparation as well as cleaning and was acquired from Millipore Q3 system having resistivity 18.2 MΩ.

8) **Glass slides:** Glass slides were used as substrate and were acquired from borosil and cut in the size of 1.6 cm X 2.6 cm. Thickness of the slide is 1.25 mm.

4.2 Methods

The following methods were adopted to perform the experiments

4.2.1 Cleaning of trough and barriers

Trough and barriers were cleaned using methanol followed by propane-2-ol and then rinsed with double distilled water followed by triple distilled water.

4.2.2 Preparation of stearic acid solution

0.1 mg/ml solution of stearic acid in chloroform was used for forming the stearic acid monolayers.

4.2.3 Preparation of subphase (zirconyl chloride solution)

0.08 mM of zirconyl chloride solution in DI Water was used as subphase. Its pH was modified using 0.1M NaOH (in required amount). It should be noted that zirconyl solution was always maintained below 23 ^{0}C as it is unstable above it.

4.2.4 Cleaning of substrate

Piranha cleaning method was used to clean the substrates, followed by sonication using DI water.

4.2.5 Preparation of Langmuir monolayer

30 microliters of stearic acid solution was added dropwise on to the subphase surface with the help of Hamilton microsyringe. It takes 15 minutes for the chloroform to evaporate and then compression process was started. The parameters for taking isotherms were: speed 10 mm/min, subphase temperature 20 $^{\circ}$C. For hysteresis measurement, pH was maintained at 7.3 and no. of cycles were 10 and other parameters were same.

4.3 Deposition of Langmuir-Blodgett film

Monolayer of tailored stability formed at the subphase surface was deposited on the glass substrate by dipper mechanism. The dipper speed was 10 mm/min for both up and downstroke with a wait of 1 minute at the top for the substrate to be dry.

4.3.1 Drying and calcination protocol

After depositing thin film on glass substrate, for drying :

1. it was dried for 30 minutes in vaccum desiccator
2. Heated at 120 ^{0}C for 1 hour for complete drying

For final phase formation

Step1:- Heat from room temperature to 380 ^{0}C at 5 ^{0}C/min. and maintained at 380 ^{0}C for 1 hour to decompose stearic acid completely.

Step2:- Heat from 380 ^{0}C to 600 ^{0}C at 5 ^{0}C/min. and maintained at 600 ^{0}C for 6 hours.

Stepped heating protocol is followed from earlier experimental work [7]

Table 4.1 Showing the data of no. of deposited layers at different pH

Sample name	pH	No. of layers
73Zr05	7.3	5
73Zr09	7.3	9
73Zr14	7.3	14
73Zr20	7.3	20
79zr10	7.9	10

4.4 Characterization Techniques

4.4.1 Surface Pressure-Area isotherms: The most basic and necessary characterization for LB thin films is π-A isotherms. Surface pressure-area isotherms were already discussed in section 2.3. In the present system, the monolayers have been characterized for understanding the effect of pH (at 3.7, 6.4, 7.3, 8.3).

4.4.2 Hysteresis

To study the stability of the monolayer, hysteresis curves were taken with 10 number of cycles.

4.4.3 Oscillating barriers

The mechanical properties of the monolayer formed had been studies of barrier oscillations. Barrier oscillation has already been discussed in section 2.6. In the present study, the properties of the monolayers were characterized at different :

a. Oscillation frequency (at 10,25,30,35,40,45,50,55 mHz)

b. Subphase pH (at 6.3, 7.3, 8.3)

4.4.4 X-ray diffraction

X-ray crystallography determines that in a crystalline state, how the atoms are closely packed. From XRD, we can determine the phase, shape, size, atomic spacing and orientation, bond angles. In XRD pattern, The intensity of diffraction peaks were recorded with diffraction angle 2θ. The analysis is based on the fact thaT X-rays interfare constructively. From Bragg's law

$$2d\sin\theta = n\lambda \quad \text{.....(4.1)}$$

Where, n = an integer, d = interplanar distance, θ = diffraction angle, λ = wavelength of x rays

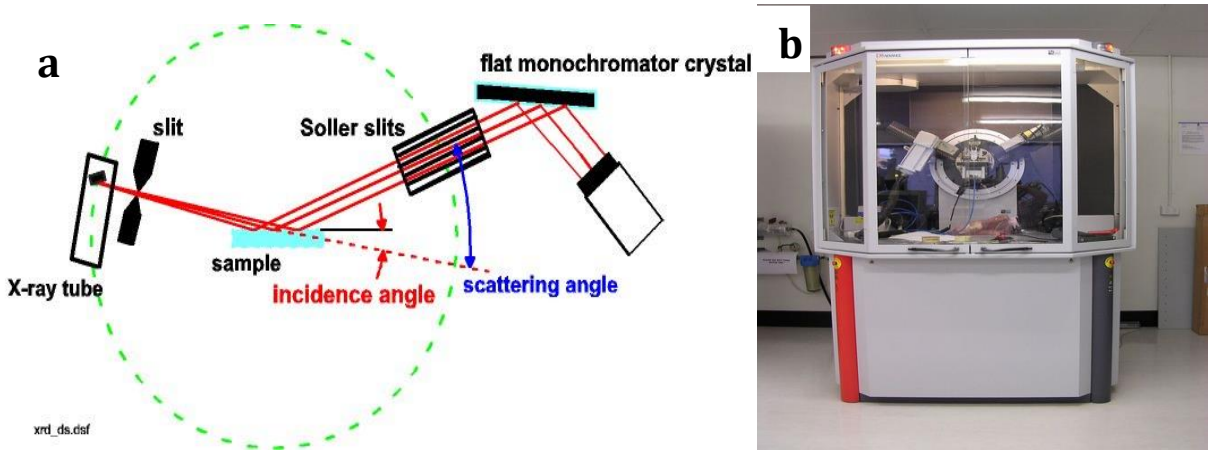

Fig 4.2 (a) Schematic of XRD [2] (b) Laboratory view of XRD

4.4.5 Field emission scanning electron microscopy (FE-SEM)

Field emission scanning electron microscopy (FE-SEM) gives morphologicall and elemental information at magnifications of about 10x to 300,000x. Comparing with conventional SEM, FE-SEM gives more clear and less electrostatically distorted image with a 3 to 6 times better spatial resolution. FE-SEM gives high-quality, low-voltage images without electrical charging of the sample**.** In lens FE-SEM is used generally for ultra high magnification of image.

In FE-SEM, electrons are used instead of light. The ejection of these electrons is done by field emission source. In FESEM, for the ejection of electrons, a cold source is used (fig 4.3). For the production of FESEM image, the electron beam sweeps across the area being

inspeting, producing many signals. The signals produced are then analyzed and transformed into the images of the topography, then the image can be seen.

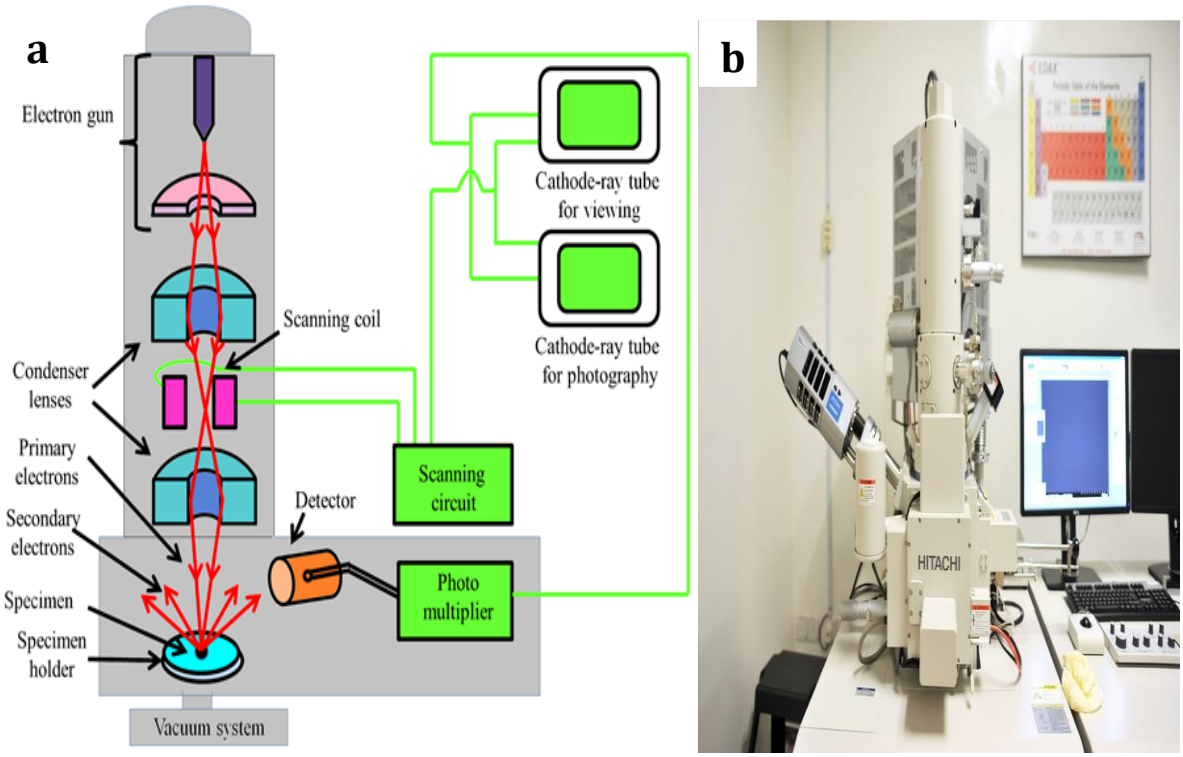

Fig 4.3 (a) Schematic diagram of FE-SEM device [3] (b) Laboratory view of FE-SEM device

We have used HITACHI SU8010 Field Emission Scanning Electron Microscope for FE-SEM studies.

4.4.6 Energy dispersive spectroscopy (EDS)

It is an analytical technique used for the elemental analysis of any sample. Since every element posess a unique atomic structure allowing a unique set of peaks on its electromagnetic emission spectrum [6]. X-rays or high energy electron beam is used for EDS. The principle of EDS is shown in fig 4.4.

We have used the Oxford INCAx-act for energy dispersive spectroscopy

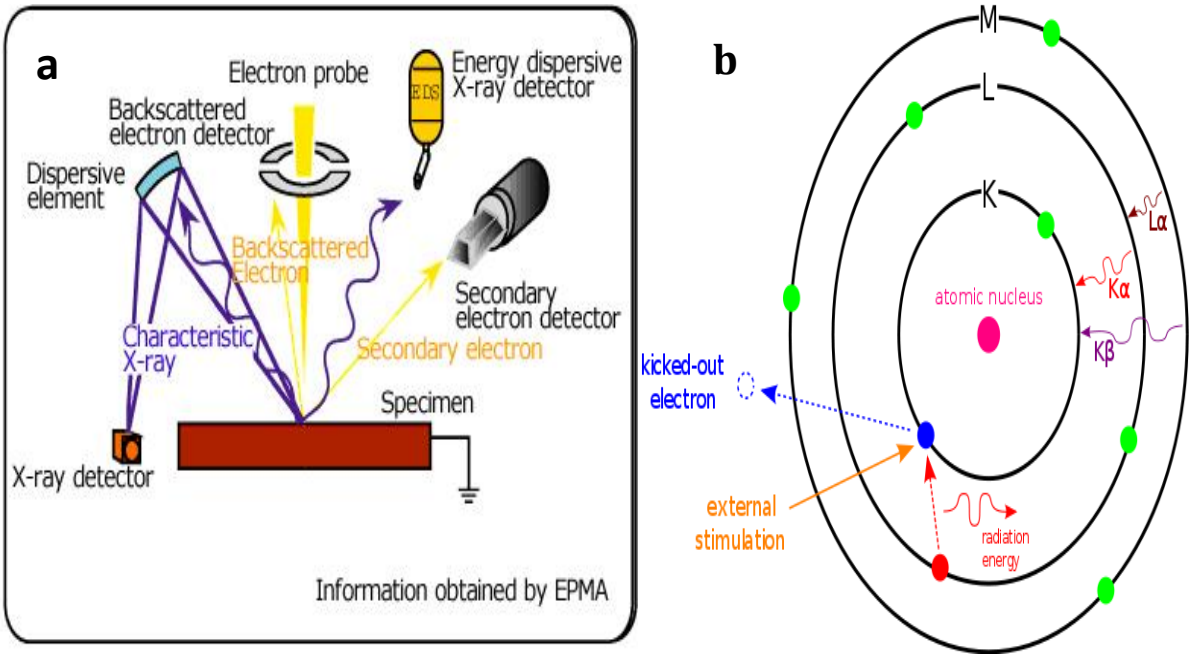

Fig 4.4 (a) Schematic of EDS [3] (b) Diagram showing the principle of EDS [4]

4.5 References

1. Sharma Rajni, Sharma Puneet (Guide), Brar Loveleen Kaur (Guide),Synthesis of Zirconium Oxide Thin Films by using Langmuir-Blodgett Technique, Masters theses@SPMS, TuDR, (2016)
2. Cullity, B. D. 1978. Elements of X-ray diffraction. 2nd ed. Addison-Wesley, Reading, Mass
3. Sam Zhang, Lin Li, Ashok Kumar, Materials Characterization Techniques, December 2008 by CRC Press
4. Joseph Goldstein (2003). Scanning Electron Microscopy and X-Ray Microanalysis

Chapter 5

Results and discussion

Overview

This chapter deals with the experimental results obtained from the characterization techniques such as π-A isotherms, hysteresis, oscillating barriers, field emission scanning electron microscopy, electron dispersive spectroscopy, XRD.

5.1 Surface pressure area isotherms

To characterize the Langmuir monolayers formed on the air-liquid interface, π-A isotherms are the most common tool. The subphase temperature was kept at 20 °C and the zirconyl chloride solution subphase concentration was $0.08x10^{-3}$mol/lt. while taking the data in the present work.

The elasticity of the monolayer can be determined from the π-A isotherm, which is reverse of compressibility as discussed in section 2.4[2]:

$$\mathbf{E= -A}\frac{\boldsymbol{d\pi}}{\boldsymbol{dA}}\text{(mN/m)} \qquad \text{……..(5.1)}$$

The above elasticity was determined from the instantaneous deformation of monolayer, thus it is free of any dissipative effect and is termed as the static elasticity of the monolayer.

5.1.1 Effect of subphase pH: The π-A isotherms for stearic acid (SA) on the surface of deionized (DI) water and $ZrOCl_2$ solution for different pH values is shown in Fig 5.1. The mean molecular area (Mma) of solid and liquid phases for each isotherm is given in table 5.1. Static elasticity was also calculated for the monolayers in the solid phase.

We know from literature that as the pH of the subphase increases, more and more positive ions in the subphase can get incorporated into the SA monolayer leading to formation of SA and ion-stearate mixed monolayers [1, 3]. For divalent ions this gives monolayers of better compaction with decreased Mma i.e. monolayers of high density [1, 2, 3]. From the data it is clear that at pH 3.7 the isotherm behavior is a signature of the behavior of SA at low pH than any zirconyl ion (ZrO^{2+}) incorporation [4]. As the pH is increased the ZrO^{2+} ion incorporation in the monolayer starts. At pH 6.4 the isotherm shows an increased Mma and

higher elasticity indicating that the incorporation of the Zirconyl (ZrO^{2+}) ion has started resulting in disruption of the SA monolayer close packed structure. A further increase in pH to 7.3 results in enhanced incorporation of ZrO^{2+} ions as indicated by a decrease in the Mma and enhanced static elasticity of the solid phase. A further increase in pH results in enhancement of Mma and reduction of elasticity indicating an opening up of the Zirconyl-stearate (ZrO-stearate) monolayer structure due to repulsion between the ZrO^{2+} ions. Inset in fig 5.2 shows the variation of elasticity of the solid phase for the pH 7.3 and 8.3 isotherms. It is very clear from the graph that the value of static elasticity for the pH 8.3 sample increases rapidly and then slowly falls off. This behavior is very different from that for pH 7.3 where the increase as well decrease happens at nearly same rate. It is believed that the fall in elasticity is slower in case of pH 8.3 sample since the monolayer has an open structure so as a result the final breakdown of the monolayer is not as abrupt.

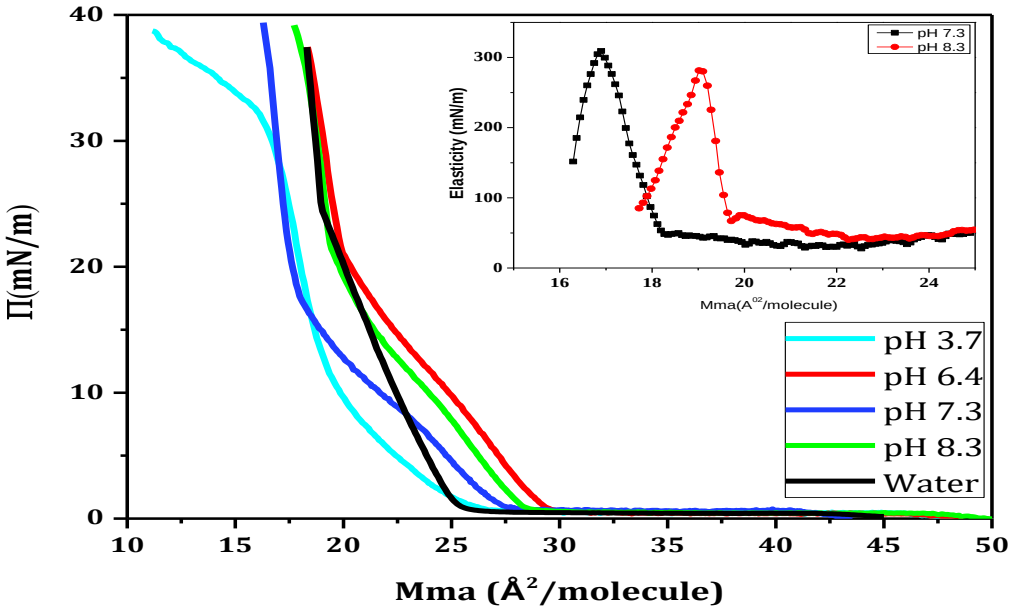

Fig 5.1 π-A isotherms of stearic acid on DI water and $ZrOCl_2$ solution for different sub-phase pH values**.** Inset shows the variation of the static elasticity for the solid phase of the pH 7.3 and 8.3 monolayers.

Based on these results the Langmuir-Blodgett monolayers of ZrO-stearate were deposited at pH 7.3 since for this pH we get the dense monolayer as well as large incorporation of Zr.

Table 5.1 Static elasticity and Mma of liquid and solid phases for different subphase pH values.

pH	Mma of solid phase (Å²/molecule)	Mma of liquid phase (Å²/molecule)	Elasticity (mN/m)
Water	20.0	26.4	378.4
3.7	20.8	29.9	167.3
6.4	22.2	32	230.1
7.3	19.2	30.9	309.1
8.3	21.2	31.1	281.5

5.1.2 Hysteresis

The information about the configuration retention of the monolayers is determined by hysteresis isotherms which are repeated compression and expansion cycles. The hysteresis curves for 10 cycles on a $ZrOCl_2$ solution subphase for pH 7.3 is shown in fig 5.2. The data shows the hysteresis effect i.e. the monolayer is becoming compact in successive compression cycles. Table 5.2 gives the values for the static elasticity for the solid phase as well as the Mma for the liquid and solid phases for each successive cycle. The variation of the parameters is shown in fig 5.3 (a, b).

Table 5.2 Static elasticity and Mma of liquid and solid phases for different cycles during the hysteresis experiments.

No. of cycle	Mma of solid phase (Å²/molecule)	Mma of liquid phase (Å²/molecule)	Elasticity (mN/m)
1	28.6	35.3	377.1
2	28.1	33.5	245.3
3	25.5	32.3	256
4	24.6	31.3	256.8
5	24	30.3	288.2
6	23.5	29.4	295.0
7	22.1	29.1	406.6
8	21.7	27.7	283.9
9	21.3	27.1	297.7
10	21.10	26.05	326.9

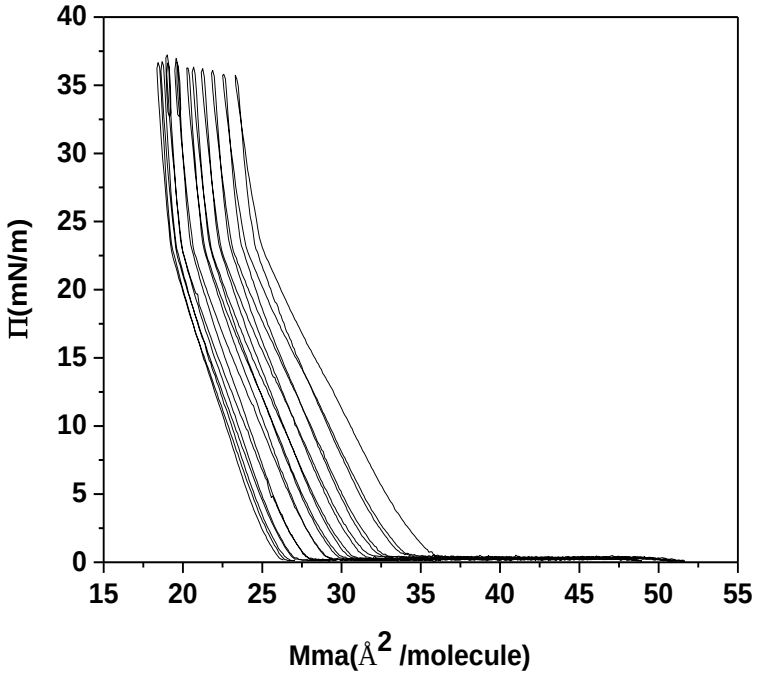

Fig 5.2 Surface pressure- area hysteresis isotherms of ZrO-stearate at pH 7.3.

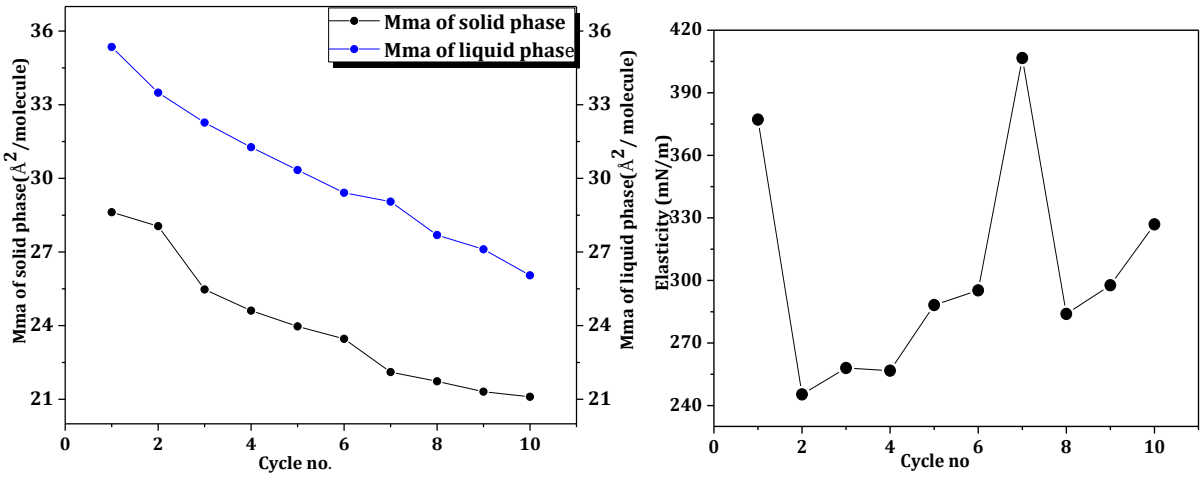

Fig 5.3 Variation of :(a) liquid and solid phase Mma, (b) Static elasticity with number of cycles

Data indicates that the as the monolayer is compressed and expanded in a cyclic fashion its Mma steadily decreases. Whereas the elasticity shows sudden fall for the second cycle and then starts increasing steadily with sudden jump followed by sudden fall at the seventh cycle followed again by steady increase. It is believed that the decrease in Mma and cycling

of elasticity happened due to the double bonded oxygen attached to the Zr atom in the ZrO^{2+} ion. This double bonded oxygen dangling from each Zr can keep changing its configuration and orientation. In the first cycle the O bonds may be increasing the size of the compacted layer due to stearic hindrance. But as the monolayer is cycled these oxygen atoms may find better stearic configuration leading to lowering of Mma. A change in configuration will also change the interactions and hence the sudden decrease in the elasticity. With more number of cycles the Mma decreases steadily which results in a steady increase of elasticity. The sudden jump in elasticity at the seventh cycle may be due to achievement of a configuration which is highly favorable for enhanced interaction. But the effect is lost when the configuration is lost during the next expansion cycle.

5.2 Oscillating barrier characterizations of ZrO-stearate monolayers

Oscillating barrier characterizations are used to determine the viscoelasticity of the monolayers. Viscoelasticity measurements inform about the interaction forces along with the relaxation processes within the films. Oscillatory barrier measurements were performed in the solid phase to study the viscoelasticity of the ZrO-Stearate monolayers layers at the surface pressure of 35 mN/m with the oscillation compression of $0.8A_0$. The isotherms were taken at the barrier speed of 10 mm/min. The viscoelastic properties such as ε (dynamic elastic modulus), ε_s (Storage modulus), ε_v (dissipation modulus) for each frequency were determined by inbuilt software of LB trough system.

5.2.1 Effect of barrier oscillation frequency

The time scales used in the oscillating barrier measurement are important because viscoelasticity involves the relaxation processes. In this case the oscillation of barrier was done at a range of frequencies varying from 10 mHz to 55 mHz in steps of 5 mHz. The frequency range is based on the fact that the generated wave cannot have a speed lower than the speed of the barriers and the relaxation processes will not be detectable if it is too fast. From the literature survey for similar systems the frequency range was decided upon [7]. Since the monolayers show highest static elasticity for the pH of 7.3 thus for these measurements this pH was chosen. Fig 5.4 shows the π variations during the measurement

Table 5.3 and fig. 5.5 give the viscoelastic properties data obtained by analyzing of these curves

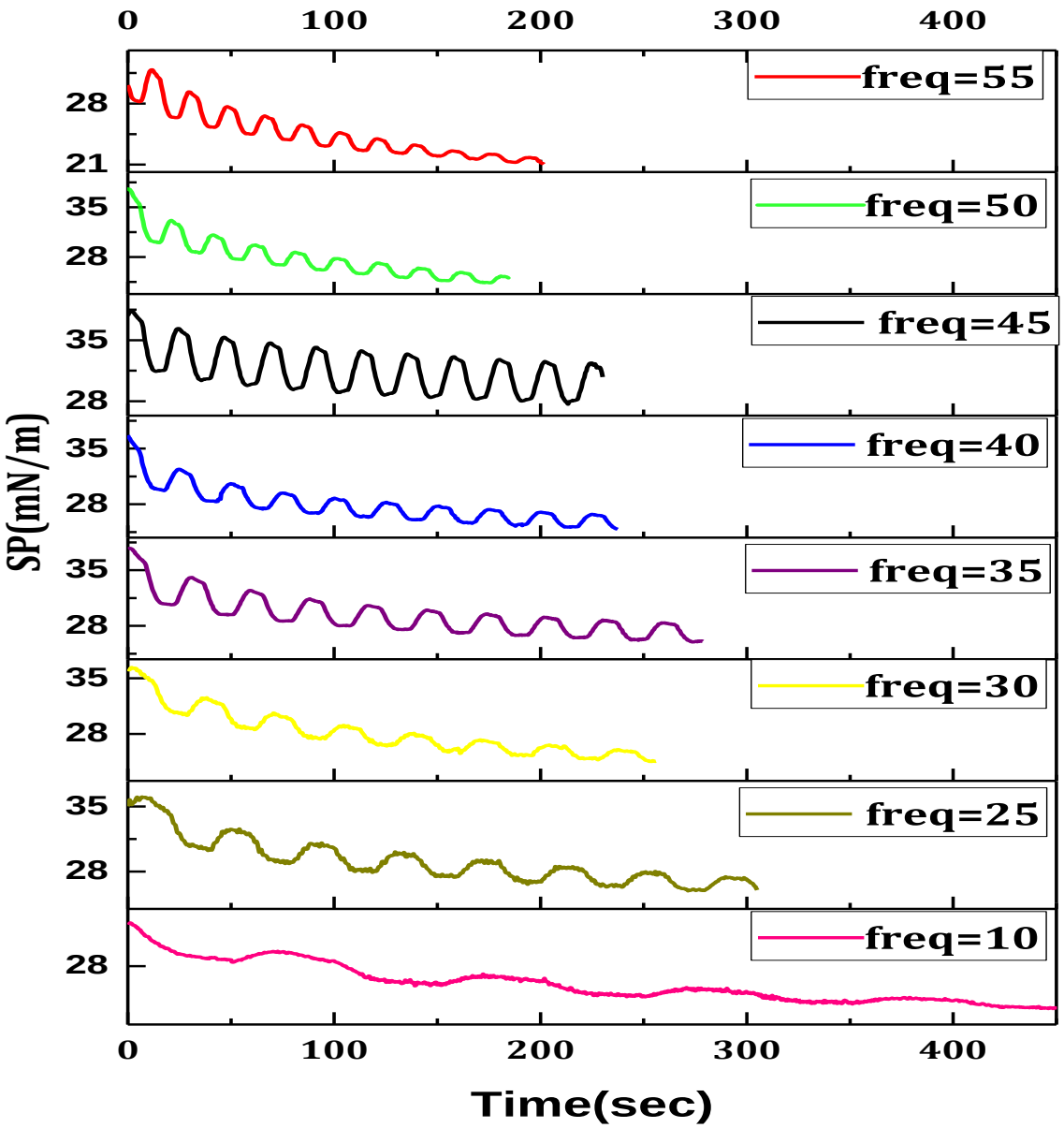

Fig 5.4 Shows surface pressure variations for barrier oscillation at different frequencies for ZrO-stearate monolayers

Table 5.3. Viscoelastic properties obtained from the analysis of curves obtained at different frequencies.

Frequency (mHz)	|ε| (mN/m)	ε_s (mN/m)	ε_v (mN/m)
10	32.5	32.4	1.9
25	46.4	44.7	12.7
30	75.7	24.1	71.8
35	389.8	151.1	359.4
40	110.1	84.6	70.5
45	159.4	153.9	41.3
50	60.6	50	34.3
55	99.3	91.3	39

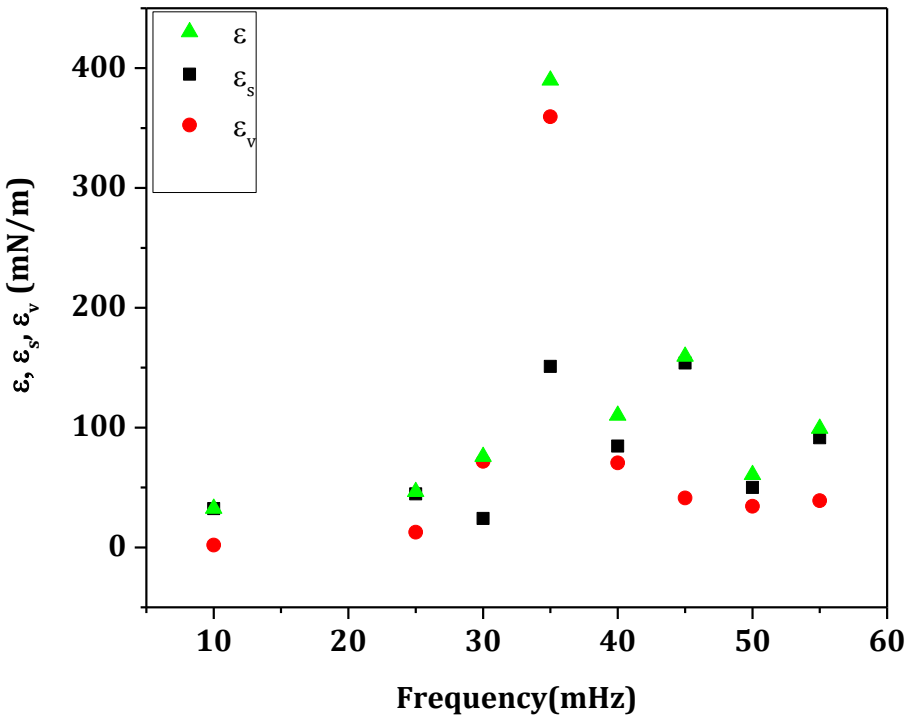

Fig 5.5 Graph showing variation of ε, ε_s and ε_v with barrier oscillation frequencies

With increase in frequency, the dynamic elastic modulus increases with maxima at 35mHZ.This is due to peaking of ε_v as well as ε_s at 35 mHz with ε_v having a large contribution. This shows that at 35 mHz, a relaxation process occurs in the film which may

be inhibiting the intermolecular interactions/structure. There is a decrease in ε_v with further increase in the frequency of oscillating barrier. From the results it is seen that the system is most stable for the barrier oscillation frequency of 45 mHz. So the effect of pH on dynamic elasticity is determined at the barrier oscillation frequency of 45 mHz.

5.2.2 Oscillation of barriers at different subphase pH

π-A isotherm analysis clearly indicates that the elastic properties of the ZrO-stearate monolayers is determined to a certain extent by the subphase pH. The oscillation of barriers was performed at 45 mHz to understand the effect of pH on the viscoelastic properties of the monolayers for different subphase pH: 6.3, 7.3, 8.3. Fig 5.6 shows the oscillations of surface pressure for different values of pH values at 45 mHz frequency. Table 5.5 and Fig 5.7 give the change in viscoelastic properties obtained by analyzing these curves.

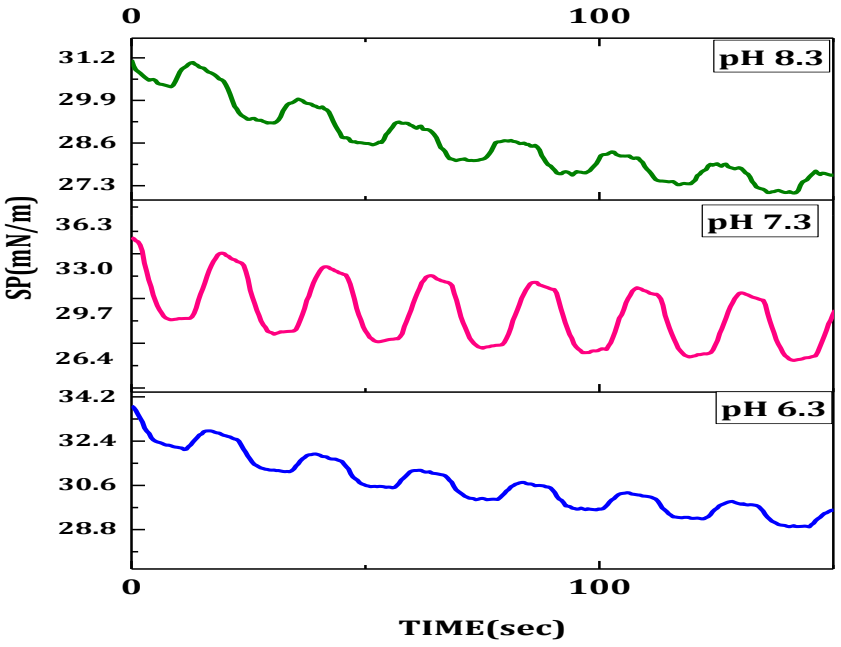

Fig 5.6 Surface pressure variations for barrier oscillation experiments for different subphase pH.

Table 5.4 Viscoelastic properties obtained from the analysis of curves obtained at different subphase pH.

pH	|ε| (mN/m)	ε_s (mN/m)	ε_v (mN/m)
6.3	14.37	14.26	1.76
7.3	159.38	153.94	41.30
8.3	57.06	-56.48	8.10

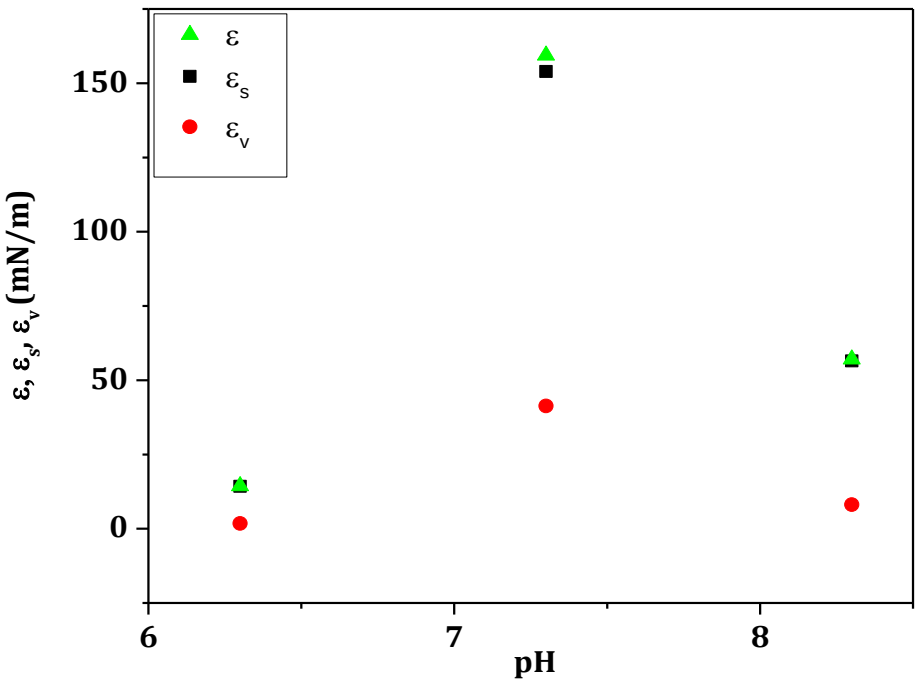

Fig 5.7 Graph showing variation of ε, ε_s and ε_v with subphase pH

5.3 Deposition of ZrO-stearate LB films

The transfer ratios (TR) of the first 10 deposition cycles for the deposition of the zirconyl stearate films on glass substrate is shown in fig 5.8. The layers were deposited on glass substrate only during upstroke which can be seen from the figure. Thus the figure clearly shows that the ZrO-stearate deposits uniformly with Z-Type configuration.

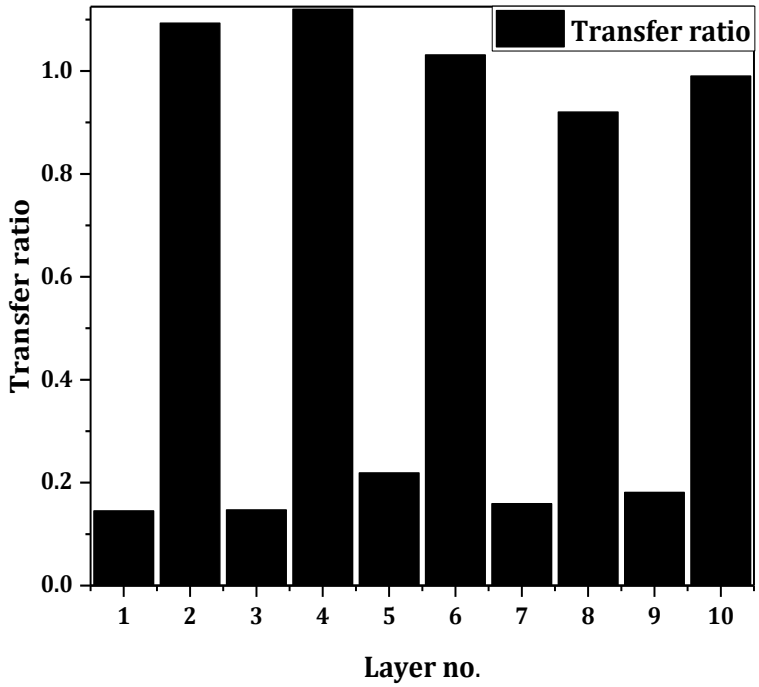

Fig 5.8 Graph shows variation of layer no. with TR

After deposition, the LB films were dried and then calcined at high temperature in a furnace for the formation of final phsae regarding the protocol discussed in section 4.3.1. On the basis literature survey, the final temperatures and times were decided [5,6].

5.3.1 Energy-Dispersive Spectroscopy (EDS)

From the EDS spectrum, the presence of Zr in the final phase formed was confirmed. The bare glass substrate was compared with that one having the film of ZrO_2. The presence of Zr in the deposited films is confirmed clearly by fig 5.9.

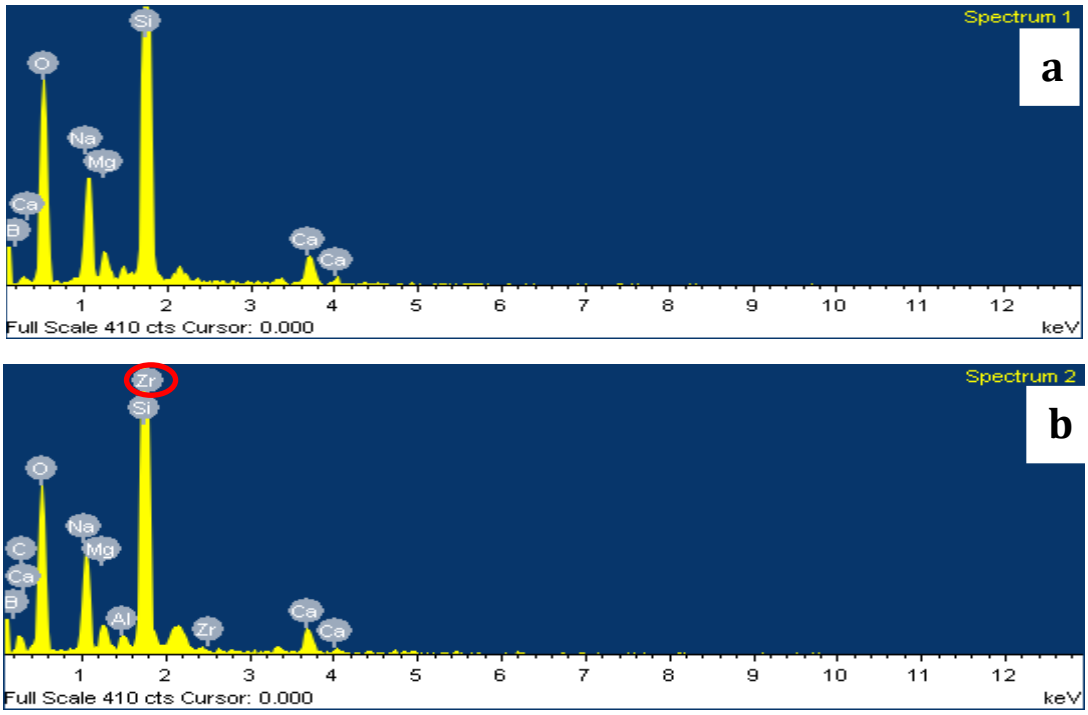

Fig 5.9 EDX pattern of (a) bare glass slide (b) glass slide with phase formed film for the 73Zr20 sample.

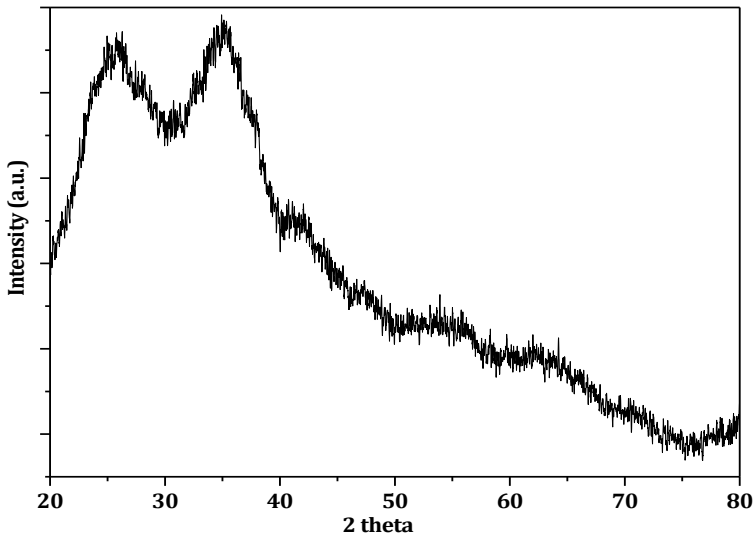

Fig 5.10 XRD pattern for the ZrO_2 thin film obtained from 20 layers ZrO-stearate LB deposition.

5.3.2 X-Ray Diffraction (XRD)

The formation of phase in the oxide films was checked using X-ray diffraction. Fig 5.10 shows the XRD pattern of 73Zr20 sample after calcination. No distinct peaks are observed but two broad humps around $2\theta \sim 30$ are observed. By comparing with earlier results in the group, it is indicated that the final phase formed is monoclinic ZrO_2 (ICDD – No: 01-074-1200) [6]. Since the thickness of film is very less, lack of distinct peaks is obvious. The thickness of the films was expected to be 10-12 nm but was not measured. The thickness is predicted on the basis of previous work, since for 200 layer deposition a film of nearly 100 nm was observed [6].

5.3.3 Zirconium oxide thin film morphology

The field emission scanning electron microscopy was used to characterize the surface morphology of the calcined films. The analysis of the images obtained was done using Axio vision SE64 Rel. 4.9.1 software and for each sample, grain size distribution was determined.

5.3.3.1 Effect of number of layers

The number of ZrO-stearate layers deposited affects the final morphology of ZrO_2 thin films that decides the amount of Zr present on the surface. Fig 5.11 gives the representative FE-SEM images and the distribution of grain size for the 73Zr09, 73Zr14, 73Zr19 samples. From the grain size distribution analysis, it is observed that Gaussian distribution is followed by the grain size for ZrO_2 thin films. Table 5.5 gives the samples details and the average grain size for each sample. By closely looking at the FE-SEM images, it is observed that the most uniform and continuous film is given by 14 layer deposition. The wider distribution of grains is observed for 09 layers and that for 20 layers enhanced granularity is observed. Thus we need to deposit 14 layers for the formation of continuous, uniform film.

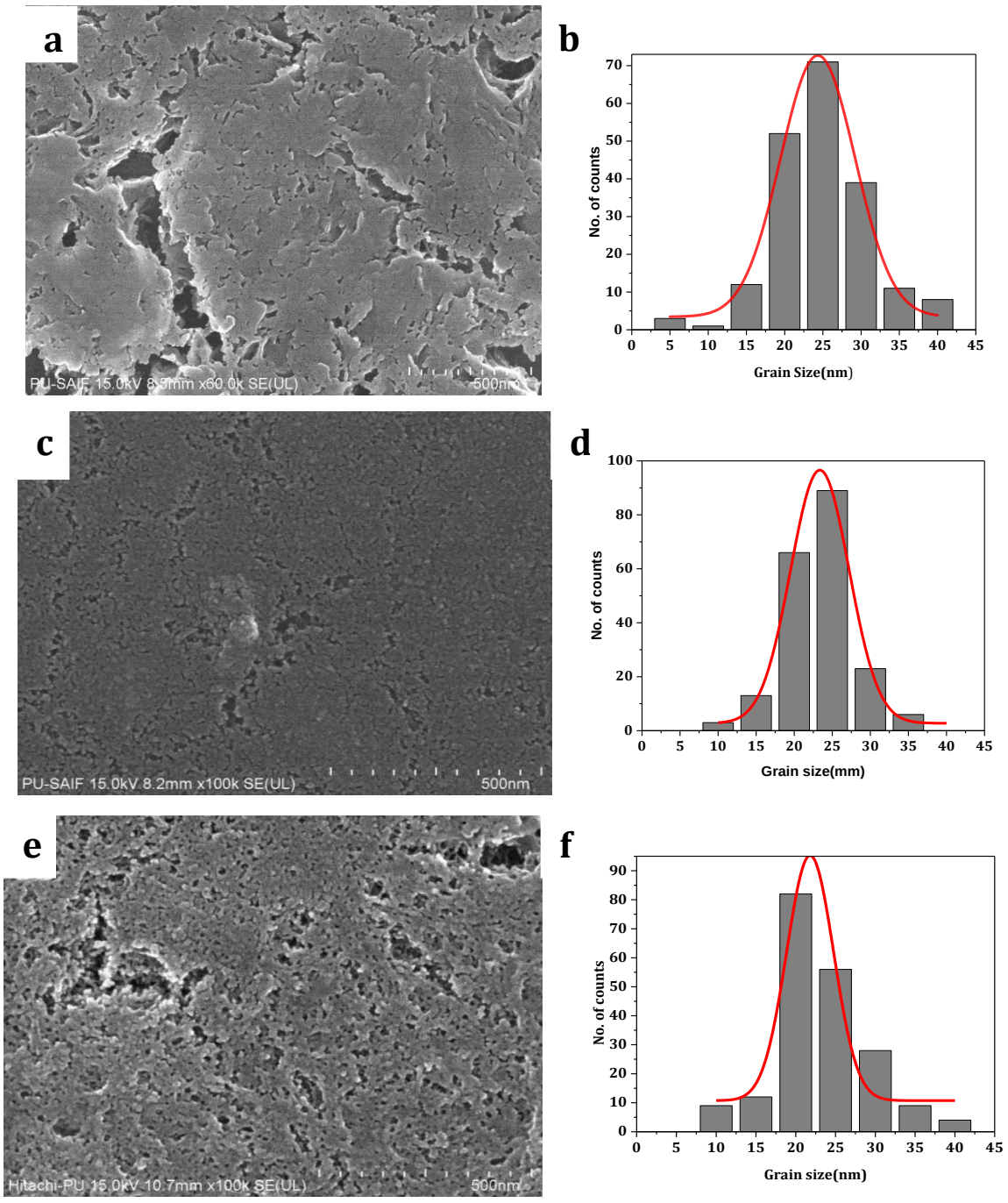

Fig 5.11 (a),(c),(e) showing FE-SEM images of the surface of the thin films of ZrO_2with9, 14 and 20 layers respectively at pH 7.3 and (b),(d),(f) shows Grain size distribution for 200 grains for 9,14,20 layers respectively

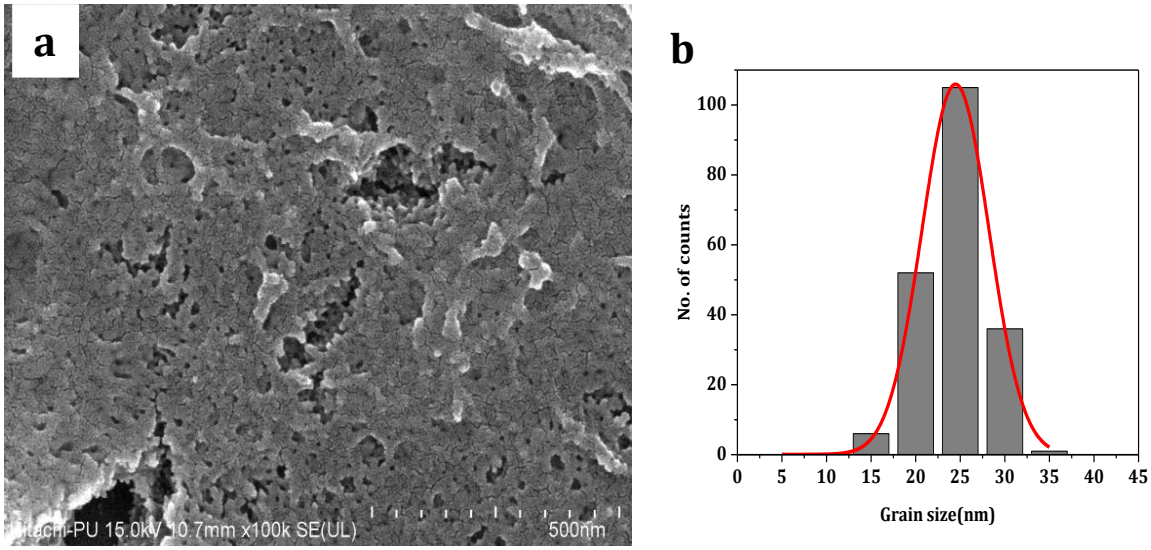

Fig 5.12 (a) FE-SEM images of the surface of the thin films of ZrO_2 with 9 layers at pH 7.9. (b) Grain size distribution for 200 grains.

Table 5.5 Shows the average grain size for 200 grains with no. of layers and pH.

Sample Name	pH	No. of layers	Grain size (nm)
73Zr09	7.3	9	23.5
73Zr14	7.3	14	23
73Zr20	7.3	20	22
79Zr09	7.9	9	25

5.3.3.2 Effect of subphase pH

The incorporation of zirconyl and the layer compaction of the zirconyl-stearate monolayers are affected by the pH of the subphase. The zirconium atom distribution and hence the final films morphology is affected by both these two factors. LB films were deposited at different subphase pH, to understand the pH effect on the morphology. The number of layers transferred was 09. One problem faced during the LB deposition of different subphase pH was that the TR was very poor (0.5-0.7) for low elasticity samples namely 6.4 and 8.4. It is believed that this may have happened due to low compaction of the monolayers at these pH coupled with Z-type nature of LB transfer for the ZrO-stearate monolayers. These samples

were not calcined or analyzed further. Fig 5.12(b) shows the FE-SEM image with respective grain size distribution for the 79Zr09 sample. From the analysis of the grain size distribution it is noted that the grain size follows Gaussian distribution. Table 5.5 gives the sample details and the average value of grain size for the sample. A comparison of data clearly shows that for pH 7.9, the films have larger grain size which will be expected as they have more Zr incorporation. And at the same time, the films are more granular and uneven at local level. This may be the result of lower elasticity which may have resulted in stretched out LB films after deposition. So for the formation of continuous and uniform films the pH of 7.3 should be preferred.

5.4 References

1. R. K. Nath, A. Chakraborty, S. A. Husain, *Surf. Rev. Lett,* 21(2014), 1450049
2. G. Roberts, Ed. Langmuir Blodgett films, plenum press: New York, (1990)
3. Michael C. Petty. Handbook of Langmuir Blodgett Films, Cambridge University Press,(1996)
4. C. Mc Fate, D. Ward, and J. Olmsted, *Langmuir,* 9(1993), 1036- 1039
5. C. J. L. Constantino, A. Dhanabalan, and O. N. Oliveira, *Rev. Sci. Instrum,* 70 (1999), 3674
6. Sharma Rajni, Sharma Puneet (Guide), Brar Loveleen Kaur (Guide), Synthesis of Zirconium Oxide Thin Films by using Langmuir-Blodgett Technique, (2016)
7. R. Kaur, G. K. Bhullar, and K. K. Raina, *AIP Conf. Proc,* 1536 (2013), 1377–1378

Chapter 6
Conclusion and future scope

6.1. Conclusions

In this work the thin uniform films of zirconium oxide were synthesized from the ZrO-stearate LB films. Characteristics of the Langmuir monolayers control the quality of LB films and the morphology of the final oxide thin film. ZrO-stearate Langmuir monolayers were deposited and characterized on the surface of the Langmuir trough. It was observed that at too low pH the ZrO^{2+} ions do not get incorporated in the monolayer. As the pH of subphase was increased the compaction of the film and its static elasticity in the solid phase was enhanced indicating an increase in ZrO^{2+} ion incorporation. An important result to emerge from these studies was that for very high pH (8.3) the structure of the films opens up. Analysis of π-A isotherms showed that pH 7.3 monolayer has good parameters for the LB deposition. Cyclic compression and expansion of the monolayer showed that while the Mma reduces steadily, the static elasticity of the solid phase gets cycled. This behavior can be explained on the basis of the behavior of double bonded oxygen attached to the Zr atom. The oscillating barrier characterizations of ZrO-stearate monolayers at different frequencies and pH values were recorded. This chracterization also confirmed the stability of the monolayers at pH 7.3. The LB films of ZrO-stearate were Z-type. The transparent Zirconium oxide thin films on glass substrate were synthesized by deposition of 9, 14, 20 layers of ZrO-stearate at 7.3 pH followed by drying, removal of stearate chain and calcination. The presence of Zr in the calcined films was checked by EDS. 14 layers deposited at pH 7.3 formed the best film with grain size of about 23 nm. The effect of pH on the final film morphology was determined by depositing 09 layers for 6.3, 7.9 and 8.3 pH values. The TR for the pH 6.3 and 8.3 monolayers was too low so the uniform films could not be deposited. For the pH 7.9 the deposition was possible but the final films have larger grain size and were more granular and uneven at local level.

6.2. Future scope

The effect of $ZrOCl_2$ concentration in the subphase and its effects can be studied. The origin of the hysteresis effects needs to be studied further. Surface

potential studies on the monolayers are a good tool to study the orientation of the molecules. The origin of Z-type deposition is as yet not understood. This method should also be applied for the formation of stabilized cubic zirconium oxide